

Supplementary Materials

Phenazine-Based Compound as a Universal Water-Soluble Anolyte Material for the Redox Flow Batteries

Elena I. Romadina^{1,*}, Alexander V. Akkuratov², Olja Simoska³, Keith J. Stevenson⁴

¹ Skolkovo Institute of Science and Technology, Bolshoy Boulevard 30, bld. 1, Moscow, 121205, Russian Federation; elena.romadina@skoltech.ru

² Federal Research Center of Problems of Chemical Physics and Medicinal Chemistry of Russian Academy of Sciences, Semenov Prospect 1, Chernogolovka, Moscow region, 142432, Russian Federation; akkuratow@yandex.ru

³ Department of Chemistry and Biochemistry, University of South Carolina, 631 Sumter Street, Columbia, South Carolina 29208, United States; osimoska@mailbox.sc.edu

⁴ Lomonosov Moscow State University, Chemistry Department, Leninskiye Gory 1/3, Moscow 119991, Russian Federation; kjsaustin@msn.com

* Correspondence: elena.romadina@skoltech.ru

* Corresponding author E-mail address: Elena.Romadina@skoltech.ru

Table of contents

1. Literature review.....	4
2. Experimental methods.....	7
2.1. NMR characterization	7
2.2. Melting point determination	9
2.3. H-cell tests.....	9
2.4. Redox flow battery tests	9
3. CVs of the background electrolytes	10
4. CV curves of M1 in different supporting electrolytes (long potential range).....	10
5. Pourbaix diagrams	11
6. Pourbaix diagrams: reference electrodes calibration.....	12
7. Pourbaix diagrams: proposed electrochemical mechanism and DFT calculations.....	12
8. Determination of the diffusion coefficient for M1 in 0.5 M KOH from the RDE measurements	15
9. Determination of the diffusion coefficient for M1 in 0.5 M NaCl from the RDE measurements.....	16
10. Determination of the diffusion coefficient for M1 in 0.5 M H ₂ SO ₄ from the RDE measurements.....	17
11. Determination of the standard rate constant for the M1 in 1.0 M KOH by RDE studies and Koutecký-Levich analysis.....	18
12. Determination of the standard rate constant for the M1 in 0.5 M NaCl by RDE studies and Koutecký-Levich analysis.....	19
13. Membrane resistance measurements	20
14. CV of M1 and TEMPOL in neutral conditions.....	21
15. Investigation of the h-cell with Nafion 117 membrane in neutral conditions.....	22
16. Investigation of the h-cell with Fumasept FAA-3PK-130 membrane in neutral conditions	23
17. Investigation of the h-cell with Neosepta AHA membrane in neutral conditions.....	24
18. Investigation of the RFB based on M1 anolyte in neutral conditions.....	25
19. Investigation of the long cycling stability of the RFB based on M1 anolyte in neutral conditions.....	26
20. CV of M1 and K ₄ Fe(CN) ₆ in base conditions	27
21. Investigation of the h-cell based on M1 anolyte in basic conditions upon potentiostatic cycling.....	28
22. Investigation of the h-cell based on M1 anolyte in basic conditions upon mixed potentiostatic + galvanostatic cycling	29
23. Investigation of the h-cell based on M1 anolyte in acidic conditions upon potentiostatic cycling.....	30
24. Investigation of the h-cell based on M1 anolyte in acidic conditions upon mixed potentiostatic + galvanostatic cycling	31

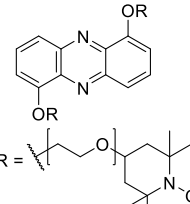
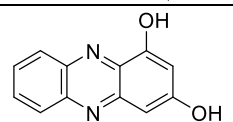
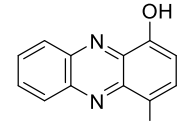
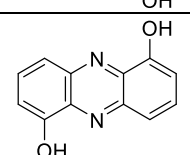
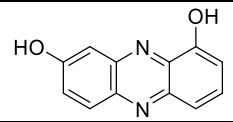
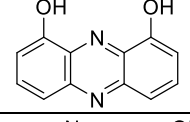
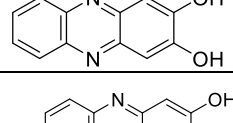
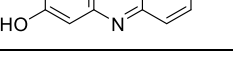
25. Investigation of the h-cell based on M1 anolyte in acidic conditions under different charge-discharge currents	32
26. Investigation of the cycling stability of the RFB with Neosepta AHA membrane in acidic conditions	34
27. Investigation of the long cycling stability of the RFB with Neosepta AHA membrane in acidic conditions	35
References	36

1. Literature review

Table S1. Summary of the investigated phenazine-based compounds, their solubilities, and literature references (SE = supporting electrolyte).

Compound	Code	Tested in	Solubility	Redox potential vs. Ag/AgCl (for water- based systems)	Best redox flow battery test	Reference		
	-	MeCN	6.8×10^{-5} M in pure water	-1.5 V vs. Ag/Ag ⁺	-	[S1,S2]		
	M1	MeCN	2.2 M in MeCN	-1.72 V vs. Ag/Ag ⁺	Anolyte – M1 Catholyte – triarylamine derivative Concentration - 0.01 M (50 cycles) SE – 0.1 M TBABF ₄	[S3]		
			1.0 M in 5.0 M TBABF ₄ in MeCN					
	BR-5	water	0.1 M in 1.0 M H ₂ SO ₄	0.0 V	Anolyte - d-BR-5 Catholyte - Ce(CH ₃ SO ₃) ₃ Concentration - 0.05 M (200 cycles) SE - 4.0 M methanesulfonic acid	[S4,S5]		
			0.054 M in 4.0 M methanesulfonic acid					
			0.34 M in 1.0 M H ₂ SO ₄	-0.013 V				
			0.206 M in 4.0 M methanesulfonic acid					
			0.11 M in 1.0 M H ₂ SO ₄	-0.012 V				
			0.175 M in 4.0 M methanesulfonic acid					
	DHP	water	0.1 M in 1.0 M NaOH	-1.02 V	Anolyte – DHPS Catholyte – K ₄ Fe(CN) ₆ Concentration - 0.1 M (200 cycles) Concentration – 1.4 M (500 cycles) SE - 1.0 M NaOH	[S1]		
	DHPC		0.95 M in 1.0 M NaOH	-1.06 V				
	DHPS		1.45 M in 1.0 M NaOH	-1.08 V				

	HP	water	1.70 M in 1.0 M KOH	-0.88 V	Anolyte – BHPC Catholyte – K ₄ Fe(CN) ₆ Concentration - 0.5 M (1305 cycles) SE - 1.0 M KOH	[S6]
	AHP		0.43 M in 1.0 M KOH	-0.99 V		
	BHPC		1.55 M in 1.0 M KOH	-0.99 V		
	2,7-DGAP 2,7-DAAP 2,7-DPAP 2,7-DBAP 1,8-DGAP 1,6-DGAP 1,6-DAAP 1,6-DPAP 1,6-DBAP	water	From 1.047 M to 0.401 M in pure water	2,7-DGAP - 0.73 V 2,7-DAAP - 0.75 V 2,7-DPAP - 0.73 V 2,7-DBAP - 0.74 V 1,8-DGAP - 0.78 V 1,6-DGAP - 0.73 V 1,6-DAAP - 0.72 V 1,6-DPAP - 0.77 V 1,6-DBAP - 0.74 V	Anolyte – 1,6-DPAP Catholyte – K ₄ Fe(CN) ₆ Concentration - 0.1 M (192 cycles) SE - 1.0 M KCl pH=12 Concentration – 0.5 M (70 cycles) SE - 1.0 M KCl pH=8	[S7]
	1,6-PFP		1.01 M in 1.0 M KOH			
	1,8-PFP		1.02 M in pure water			
	1,8-PFP		1.46 M in 1.0 M KOH			
	2,7-PFP		1.09 M in pure water			
	2,7-PFP		0.84 M in 1.0 M KOH			
	2,7-PFP		0.79 M in pure water			

	-	water + diglyme	-	-0.62 V	Anolyte – compound itself Catholyte – compound itself Concentration - 0.01 M (1800 cycles) SE – 0.5 M NaCl	[S9]
	1,3-DHP	water	0.3 M 1M NaOH 1.6 M 2M KOH	-0.81 V	Anolyte – 1,4-DHP Catholyte – $K_4Fe(CN)_6$ Concentration - 0.42 M (1000 cycles) SE - 2.0 M KOH	[S10]
	1,4-DHP		0.3 M 1M NaOH 0.5 M 2M KOH	-0.72 V		
	1,6-DHP		0.07 M 1M NaOH 0.6 M 2M KOH	-0.91 V		
	1,8-DHP		1.8 M 1M NaOH 1.9 M 2M KOH	-1.02 V		
	1,9-DHP		0.1 M 1M NaOH 0.3 M 2M KOH	-0.81 V		
	2,3-DHP		1.6 M 1M NaOH 2.0 M 2M KOH	-1.06 V		
	2,7-DHP		0.1 M 1M NaOH 0.2 M 2M KOH	-0.96 V		

2. Experimental methods

2.1. NMR characterization

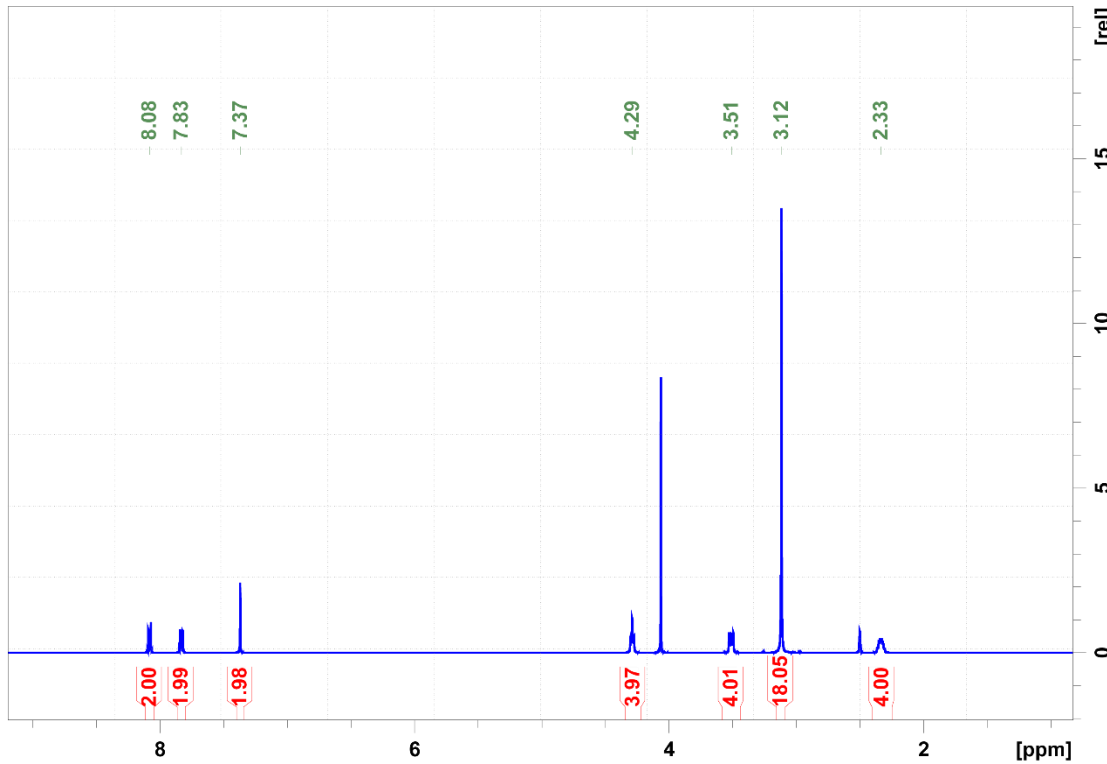


Figure S1. Full ^1H NMR spectrum of M1 compound.

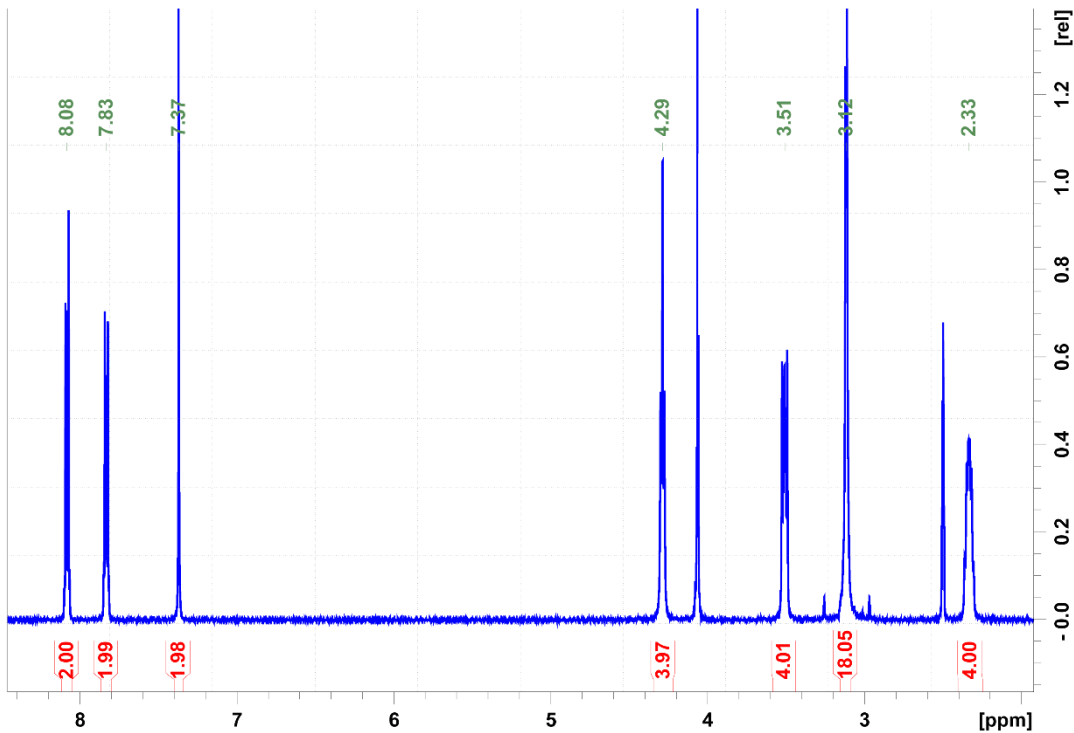


Figure S2. Zoomed ^1H NMR spectrum of M1 compound.

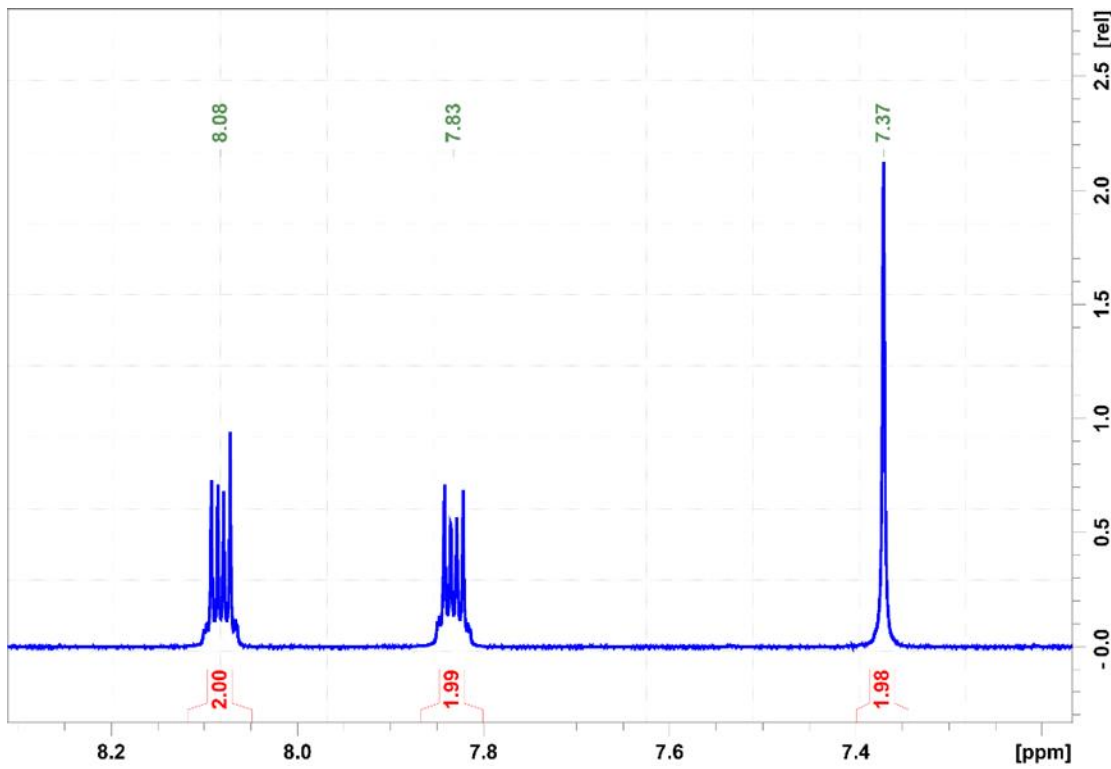


Figure S3. Aromatic region of ^1H NMR spectrum of **M1** compound.

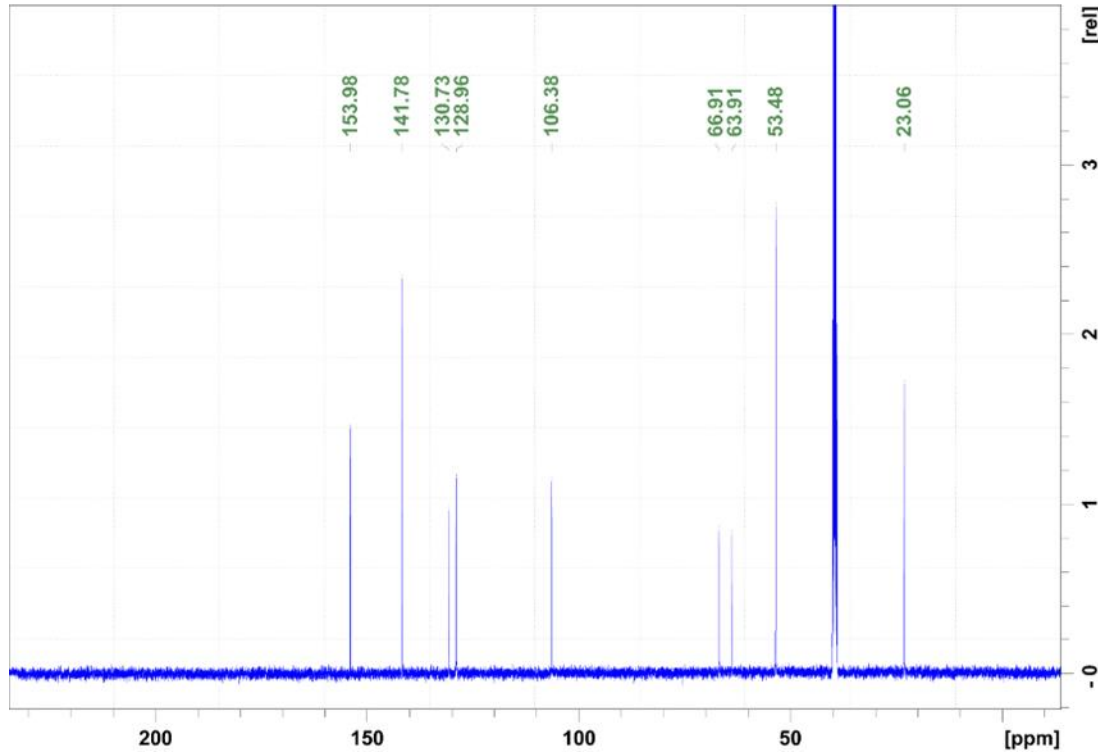


Figure S4. ^{13}C NMR spectrum of **M1** compound.

2.2. Melting point determination

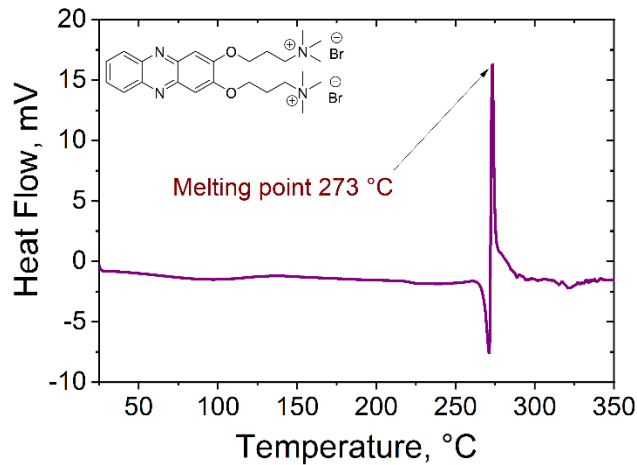


Figure S5. Differential scanning calorimetry graph for **M1** compound.

2.3. H-cell tests

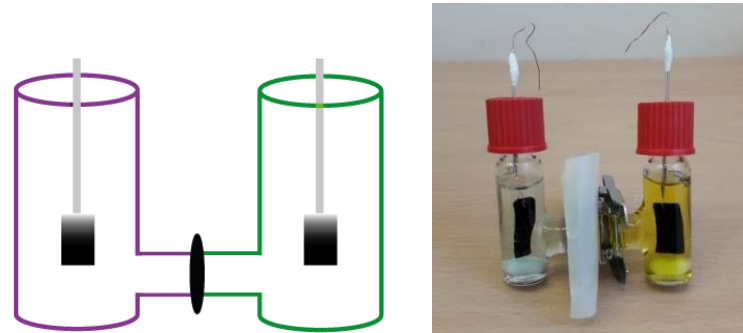


Figure S6. Schematic representation and photo of the h-cell used.

2.4. Redox flow battery tests

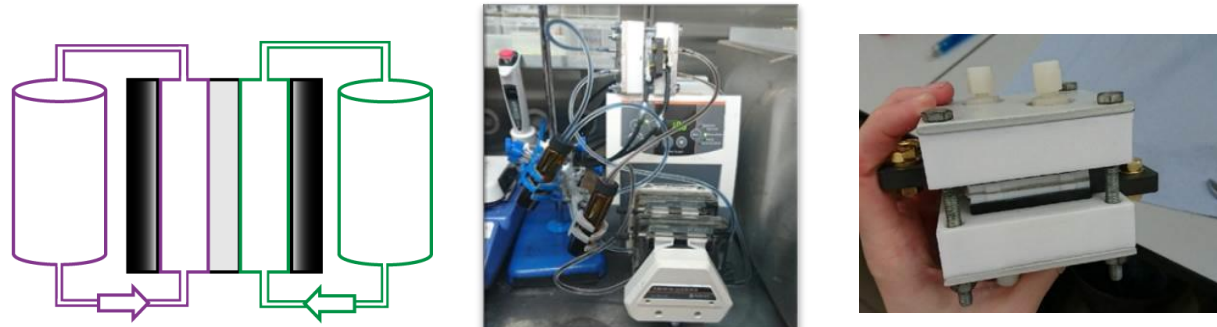


Figure S7. Schematic representation of the redox flow battery and the photos of a laboratory setup. The redox flow cell consisted of metal cell frames, Teflon cell frames, graphite/Teflon (20/80) current collectors, Teflon flow frames with graphite felt electrodes (6 mm thick graphite felt, geometric active area of 4.00 cm^2), and Neosepta AHA anion-exchange membrane.

3. CVs of the background electrolytes

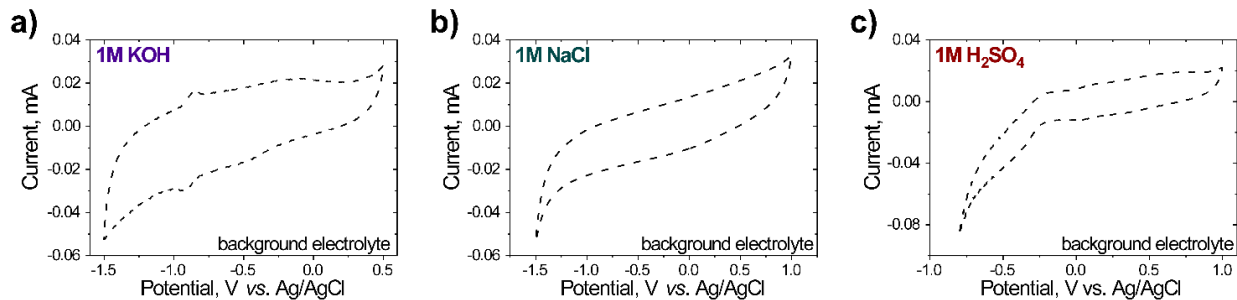


Figure S8. Cyclic voltammogram of the background electrolytes: (a) 1.0 M KOH, (b) 1.0 M NaCl and (c) 1.0 M H₂SO₄.

4. CV curves of M1 in different supporting electrolytes (long potential range)

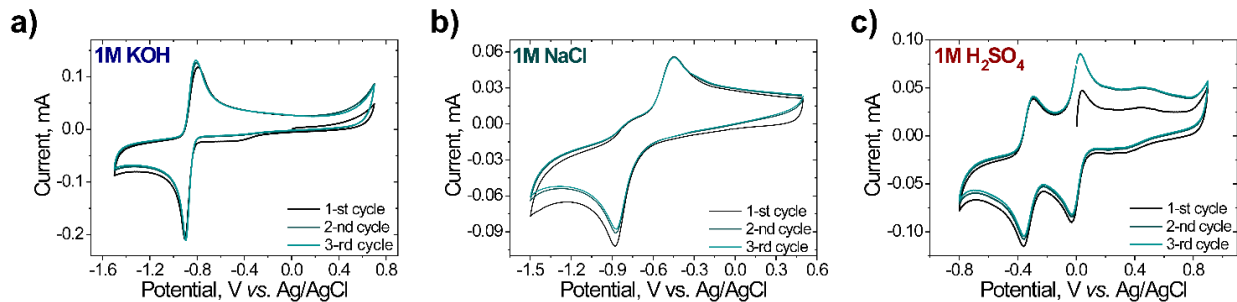


Figure S9. Cycling voltammograms were obtained for 30.0 mM aqueous solution of M1 with (a) 1.0 M KOH, (b) 1.0 M NaCl and (c) 1.0 M H₂SO₄ as supporting electrolytes at a scan rate of 100 mV s⁻¹.

5. Pourbaix diagrams

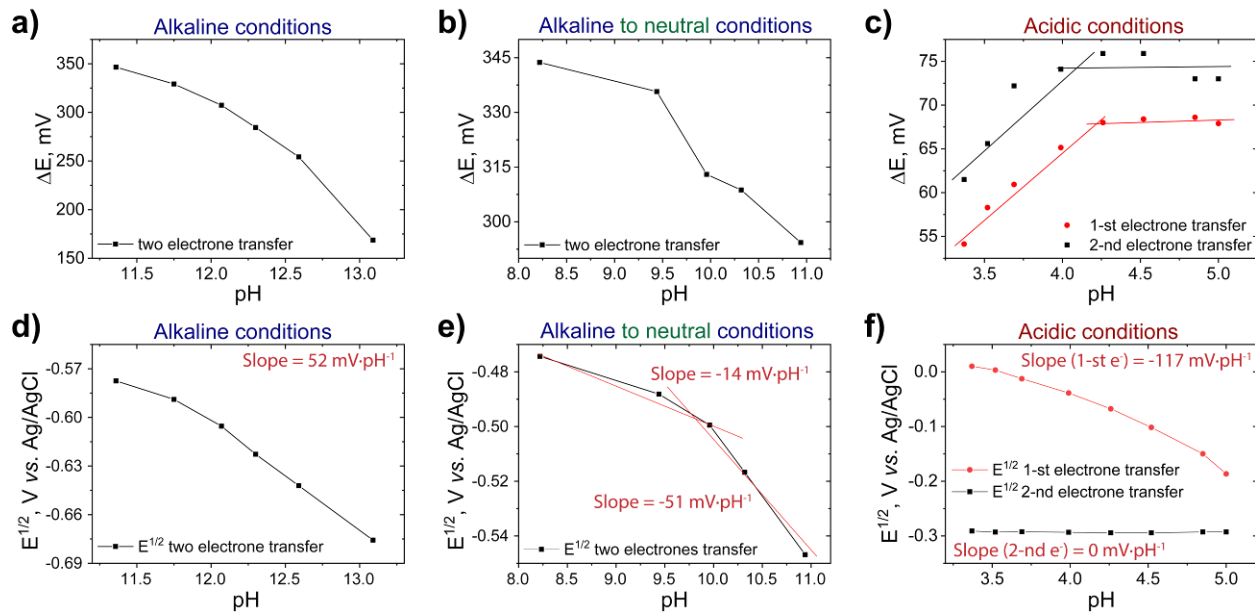


Figure S10. Dependence of peak splitting (ΔE) of the pH for **M1** in alkaline (f), alkaline to neutral (b) and acidic (c) conditions. Dependence of half-wave potential ($E^{1/2}$) of the pH for the alkaline (d), alkaline to neutral (e) and acidic (f) conditions.

6. Pourbaix diagrams: reference electrodes calibration

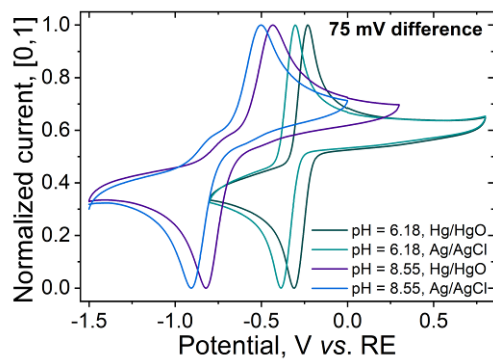
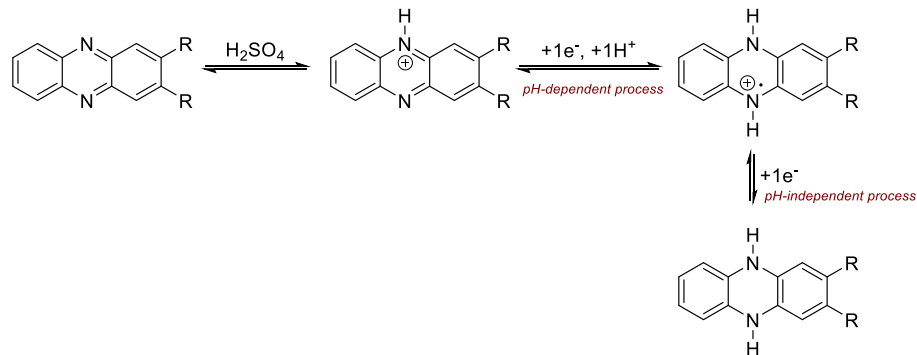


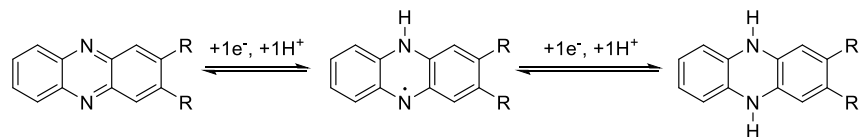
Figure S11. Calibration of Hg/HgO electrode vs. Ag/AgCl electrode. CV curves are measured for the **M1** compound at 100 mV s⁻¹ scan rate at different pH values.

7. Pourbaix diagrams: proposed electrochemical mechanism and DFT calculations

Acidic conditions



Neutral conditions



Basic conditions

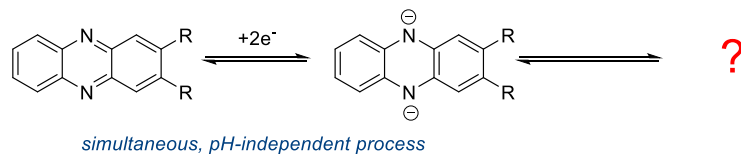


Figure S6. Proposed mechanism and thermodynamically favored protonation pathway for **M1** at acidic, neutral, and alkaline conditions.

DFT calculations - Neutral conditions

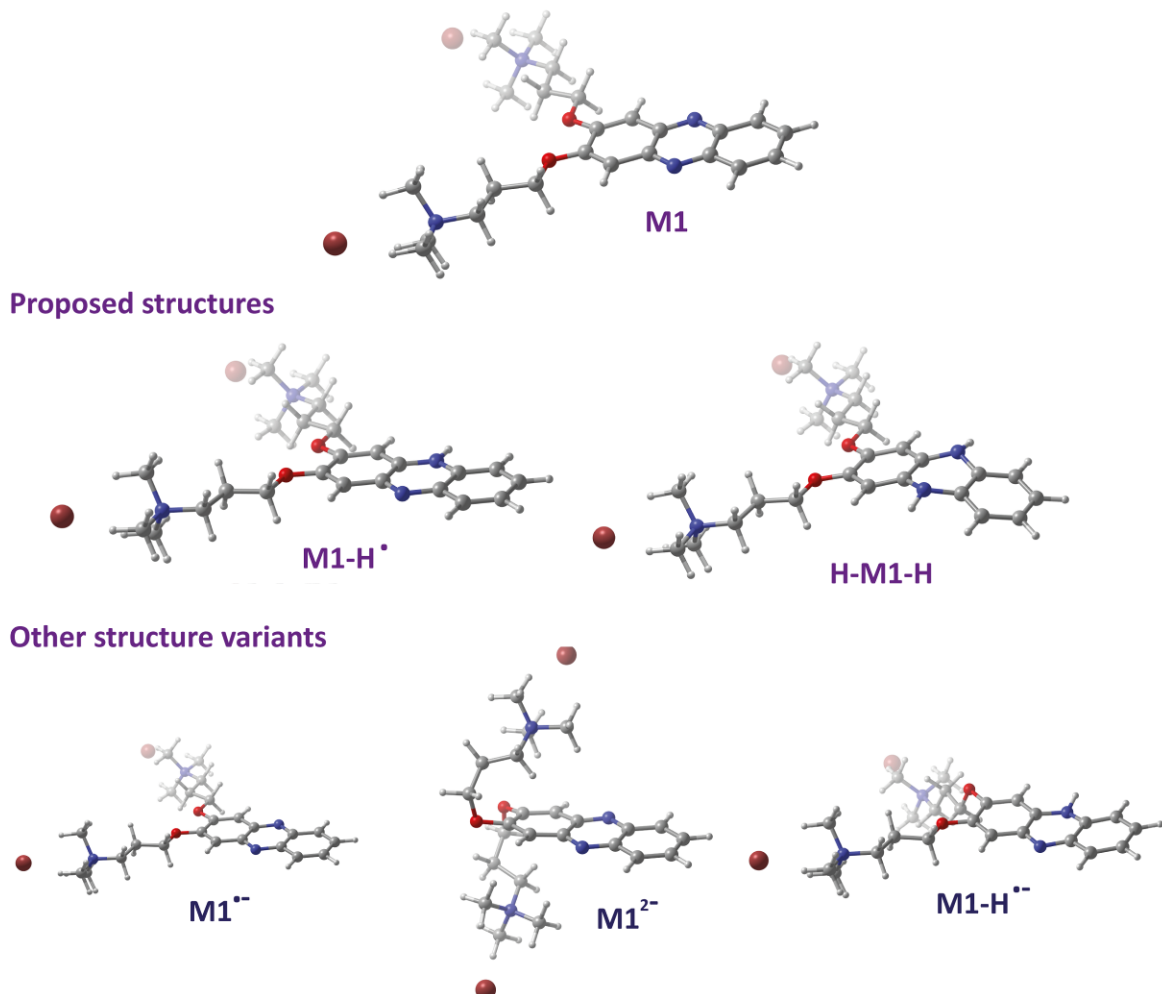


Figure S13. Optimised structures for **M1** molecule, reduced **M1-H[·]** molecule (+ 1e⁻ + 1H⁺), reduced **H-M1-H** molecule (+ 2e⁻ + 2H⁺) and other theoretically possible structure variants.

Table S2. Calculated and measured redox potentials for the **M1** reduction in neutral conditions.

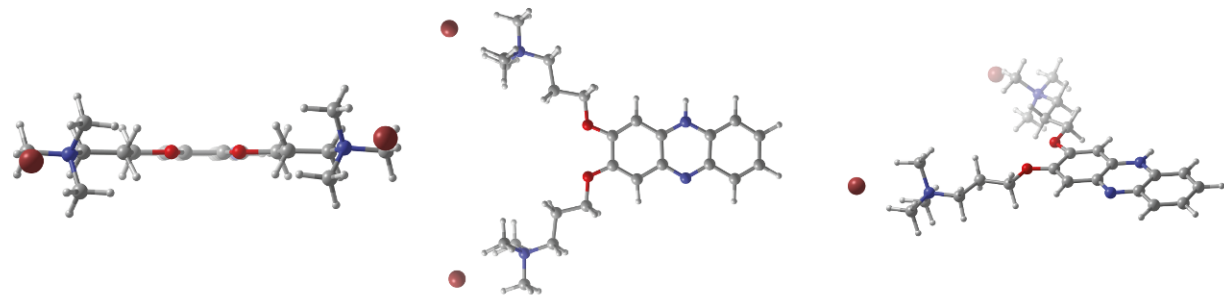
Redox process	M1 + e⁻ + H⁺ → M1-H[·]	M1-H[·] + e⁻ + H⁺ → H-M1-H
Calculated redox potential (V) vs. NHE	-0.446 V	-0.065 V
Measured redox potential (V) vs. NHE 1M NaCl Supporting electrolyte		-0.460 V

Table S3. Calculated redox potentials for other possible redox reaction for the **M1** reduction in neutral conditions.

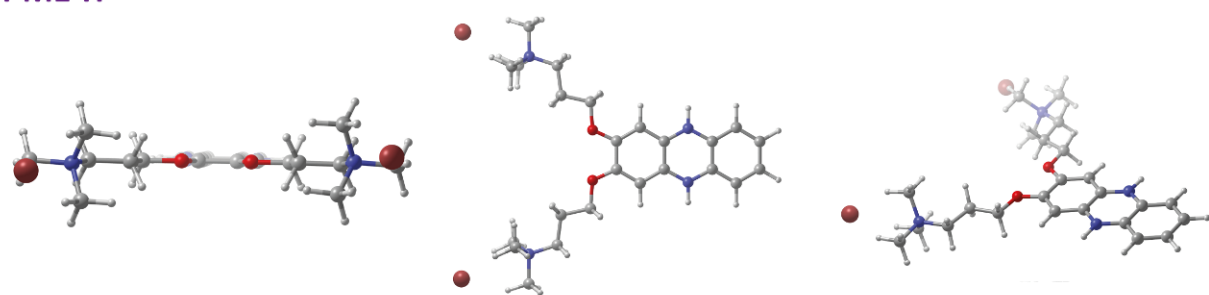
Redox process	M1 + e⁻ → M1···	M1 + 2e⁻ → M1²⁻	M1 + 2e⁻ + H⁺ → M1-H^{···}
Computed Reduction Potential vs. NHE	-2.615 V	-3.942 V	-1.422 V

DFT calculations - Acidic conditions

M1-H⁺



H-M1-H⁺



H-M1-H

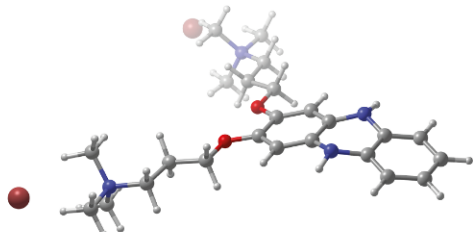


Figure S14. Optimised structures for **M1-H⁺** molecule, reduced **M1-H⁻** molecule (+ 1e⁻ + 1H⁺), and reduced **H-M1-H** molecule (+ 2e⁻ + 2H⁺).

Table S4. Calculated and measured redox potentials for the **M1** reduction in acidic conditions.

Redox process	M1-H⁺ + e⁻ + H⁺ → H-M1-H⁺	H-M1-H⁺ + e⁻ → H-M1-H
Computed Reduction Potential vs. NHE	0.298 V	-0.073 V
Measured redox potential vs. NHE 1M H ₂ SO ₄	0.26 V	-0.05V

8. Determination of the diffusion coefficient for M1 in 0.5 M KOH from the RDE measurements

The diffusion coefficient was calculated according to Levich equation for rotation disk electrode measurements. The kinematic viscosity for 0.5 M KOH solution is $1.03 \times 10^{-2} \text{ cm}^2 \text{ s}^{-1}$ [S11].

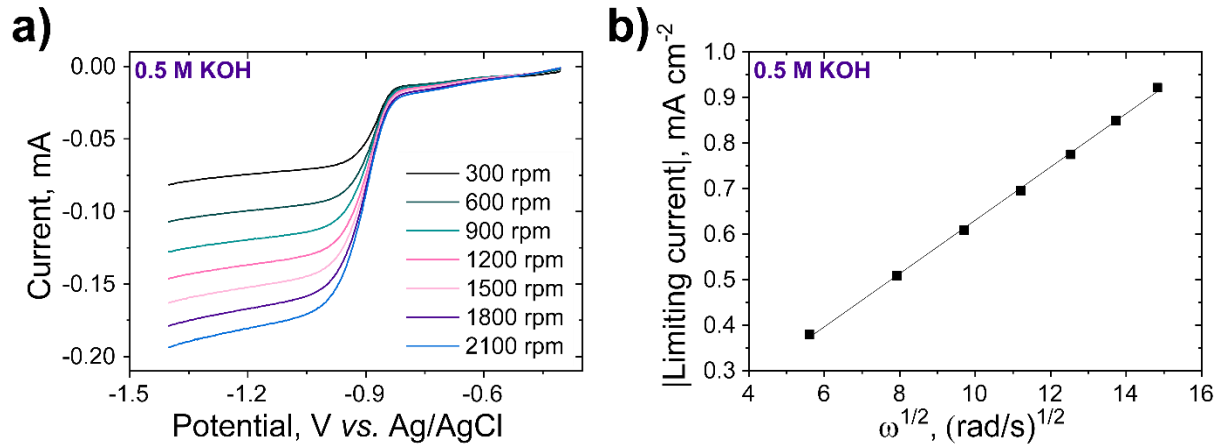


Figure S15. Linear sweep voltammetry test with a glassy carbon rotating disk electrode for **M1** in 0.5 M KOH supporting electrolyte at a scan rate of 10 mV s^{-1} (a), and linear plot of the current as a function of the square root of the rotation rate (ω) (b). Concentration of the redox-active compound was 15.0 mM.

Table S5. Data set used for limiting current - square root of the rotation rate plot and evaluation of diffusion coefficient.

ω , rpm	ω , rad s ⁻¹	Limiting current, mA (at -1.2 V)
300	31.41	-0.0745
600	62.83	-0.0998
900	94.25	-0.1195
1200	125.66	-0.1364
1500	157.08	-0.1521
1800	188.49	-0.1668
2100	219.91	-0.1809

The slopes were found to be:

Electron	Slope	Error
2 electron reduction	5.85×10^{-2}	7.68×10^{-4}

Diffusion coefficient is:

2 e reduction	
0.5 M KOH	$1.94 \times 10^{-6} \pm 2.93 \times 10^{-9}$

9. Determination of the diffusion coefficient for M1 in 0.5 M NaCl from the RDE measurements

The diffusion coefficient was calculated according to Levich equation for rotation disk electrode measurements. The kinematic viscosity for 0.5 M NaCl solution is $0.010 \text{ cm}^2 \text{s}^{-1}$ [S6].

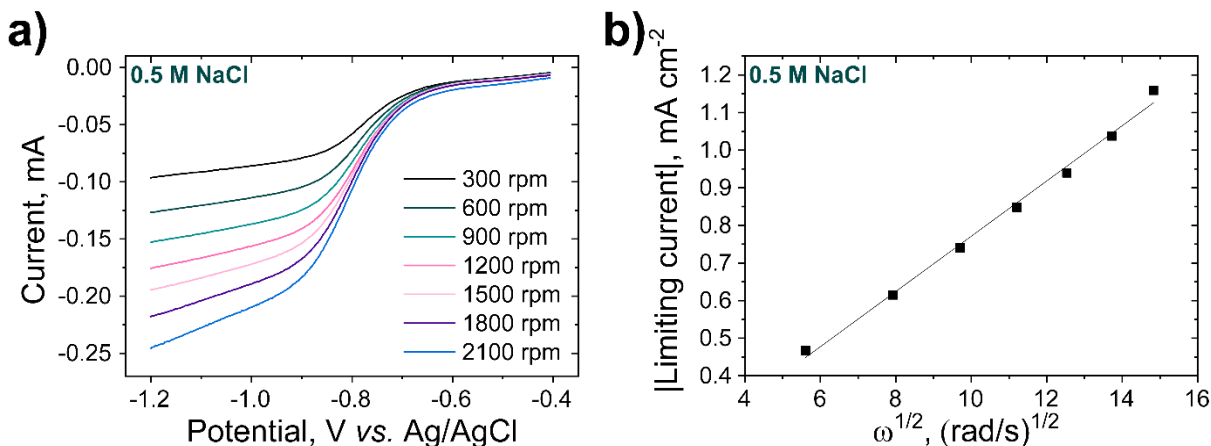


Figure S16. Linear sweep voltammetry test with a glassy carbon rotating disk electrode for **M1** in 0.5 M NaCl supporting electrolyte at a scan rate of 10 mV s^{-1} (a), and linear plot of the current as a function of the square root of the rotation rate (ω) (b). Concentration of the redox-active compound was 15.0 mM.

Table S6. Data set used for limiting current - square root of the rotation rate plot and evaluation of diffusion coefficient.

ω, rpm	$\omega, \text{rad s}^{-1}$	Limiting current, mA (at -1.1 V)
300	31.41	-0.0916
600	62.83	-0.1207
900	94.25	-0.1453
1200	125.66	-0.1665
1500	157.08	-0.1844
1800	188.49	-0.2037
2100	219.91	-0.2275

The slopes were found to be:

Electron	Slope	Error
2 electron reduction	7.45×10^{-2}	2.52×10^{-3}

Diffusion coefficient is:

	2 e ⁻ reduction
0.5 M NaCl	$9.64 \times 10^{-7} \pm 6.13 \times 10^{-9}$

10. Determination of the diffusion coefficient for M1 in 0.5 M H₂SO₄ from the RDE measurements

The diffusion coefficient was calculated according to Levich equation for rotation disk electrode measurements. The kinematic viscosity for 0.5 M H₂SO₄ solution is 0.0098 cm² s⁻¹ [S12].

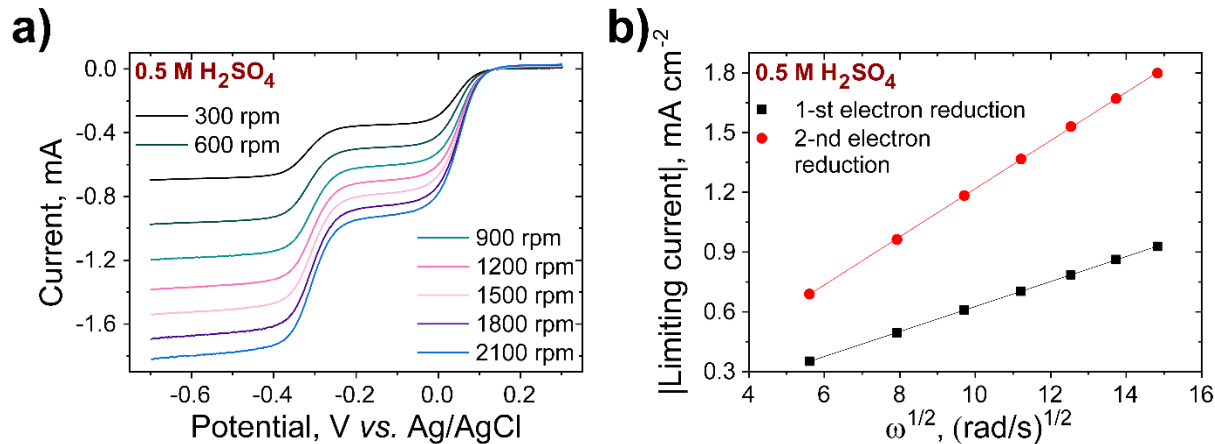


Figure S17. Linear sweep voltammetry test with a glassy carbon rotating disk electrode for **M1** in 0.5 M H₂SO₄ supporting electrolyte at a scan rate of 10 mV s⁻¹ (a), and linear plots of the currents as a function of the square root of the rotation rate (ω) (b). Concentration of the redox-active compound was 15.0 mM.

Table S7. Data set used for limiting current - square root of the rotation rate plot, and evaluation of diffusion coefficient.

ω , rpm	ω , rad s ⁻¹	Limiting current for the 1-st electron reduction, mA (at -0.15 V)	Limiting current for the 2-nd electron reduction, mA (at -0.60 V)
300	31.41	-0.351	-0.689
600	62.83	-0.493	-0.963
900	94.25	-0.609	-1.180
1200	125.66	-0.703	-1.370
1500	157.08	-0.786	-1.530
1800	188.49	-0.862	-1.670
2100	219.91	-0.927	-1.800

The slopes were found to be:

Electron	Slope	Error
1-st electron reduction	6.29×10^{-2}	2.45×10^{-4}
2-nd electron reduction	1.20×10^{-1}	4.66×10^{-5}

Diffusion coefficients are:

	1-st e ⁻ reduction	2-nd e ⁻ reduction
0.5 M H ₂ SO ₄	$2.09 \times 10^{-6} \pm 5.16 \times 10^{-10}$	$5.66 \times 10^{-6} \pm 1.35 \times 10^{-9}$

11. Determination of the standard rate constant for the M1 in 1.0 M KOH by RDE studies and Koutecký-Levich analysis

The standard electrochemical rate constant was measured by use of the Koutecký-Levich method.

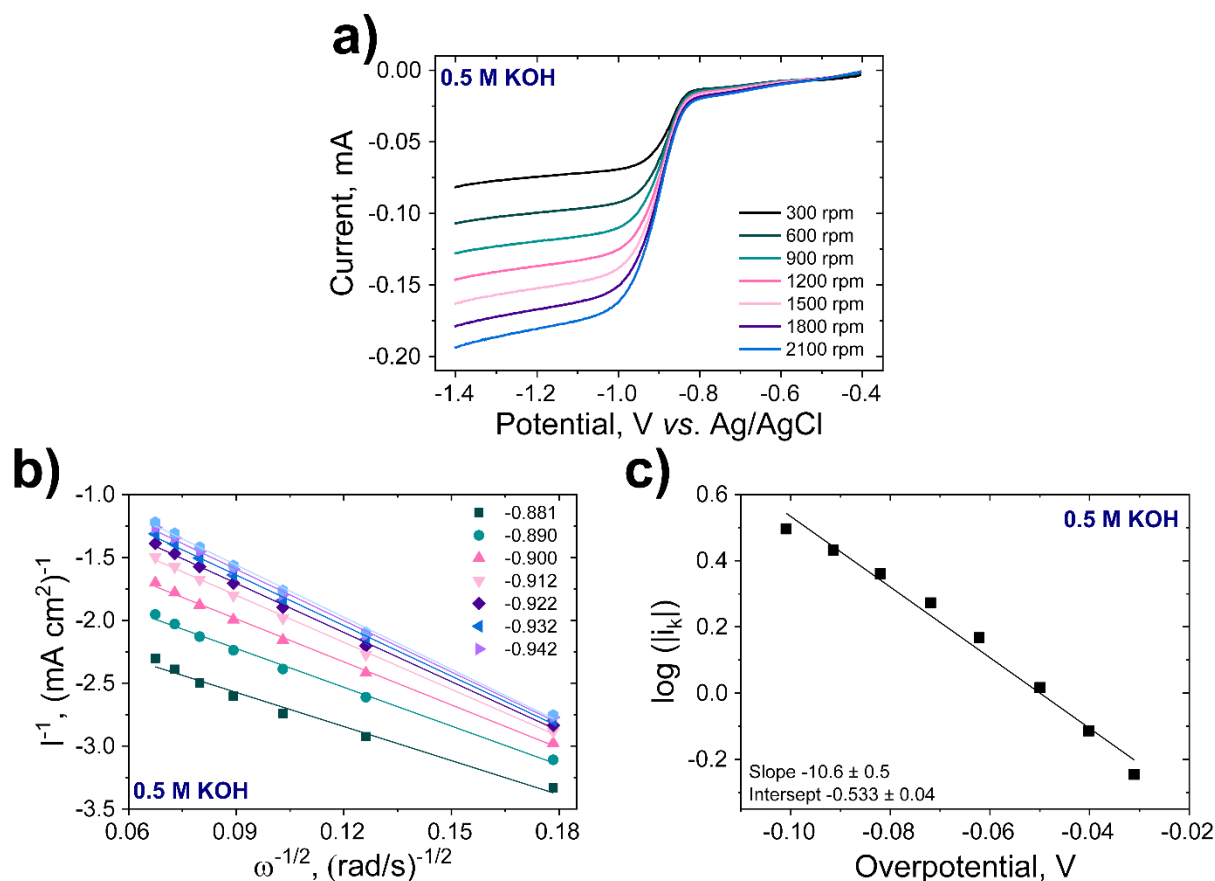


Figure S18. (a) Rotating disk electrode measurement of M1 (15 mM), 0.5 M NaCl in distilled water, scan rate 10 mV s⁻¹, rotating rates from 300 to 2100 rpm; (b) Koutecký-Levich plot for different overpotentials yielding the mass-transfer-independent current i_0 ; (c) Tafel plot yielding $k_0 = 5.16 \times 10^{-4}$ cm s⁻¹ and $\alpha = 0.90$.

12. Determination of the standard rate constant for the M1 in 0.5 M NaCl by RDE studies and Koutecký-Levich analysis

The standard electrochemical rate constant was measured by use of the Koutecký-Levich method.

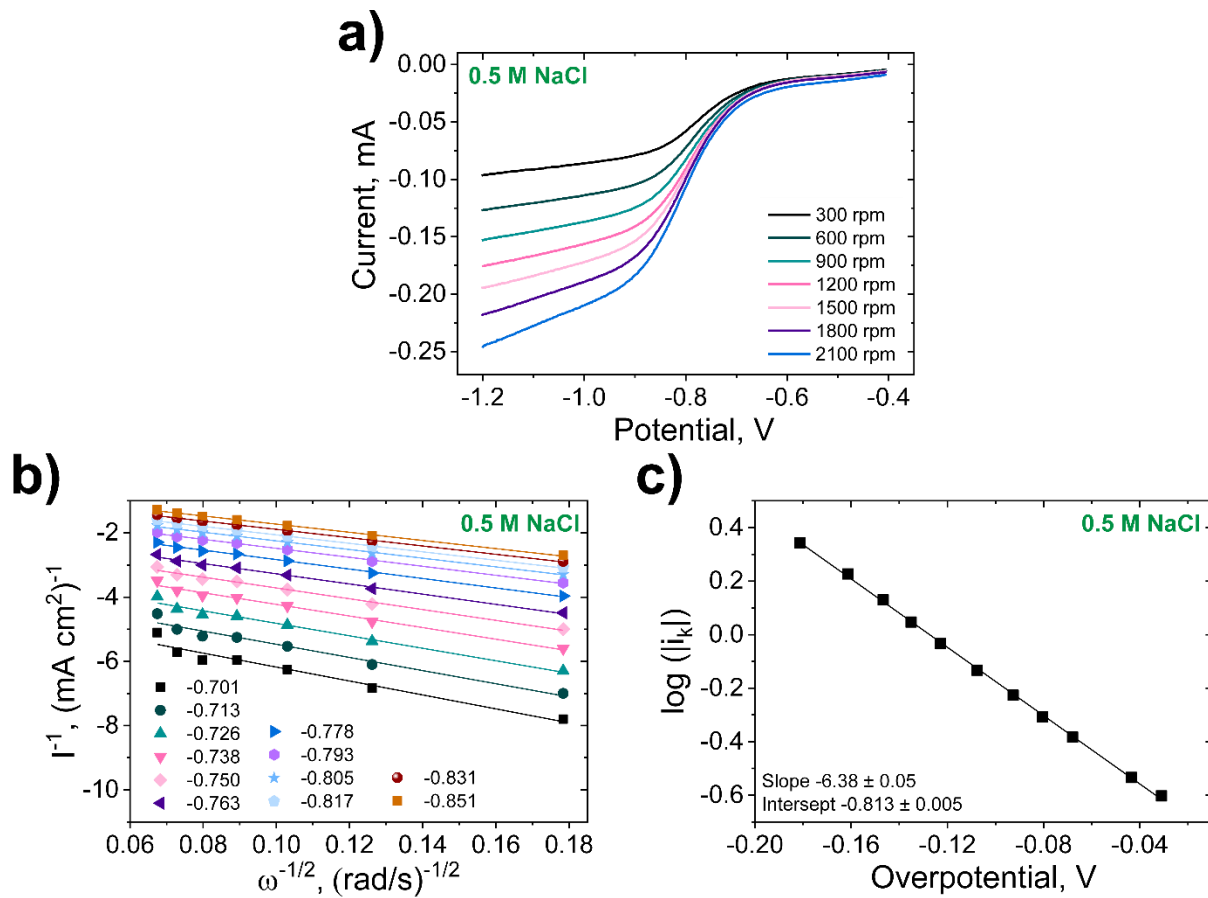


Figure S19. (a) Rotating disk electrode measurement of M1 (15 mM), 0.5 M NaCl in distilled water, scan rate 10 mV s⁻¹, rotating rates from 300 to 2100 rpm; (b) Koutecký-Levich plot for different overpotentials yielding the mass-transfer-independent current i_k ; (c) Tafel plot yielding $k_0 = 2.59 \times 10^{-4}$ cm s⁻¹ and $\alpha = 0.94$.

13. Membrane resistance measurements

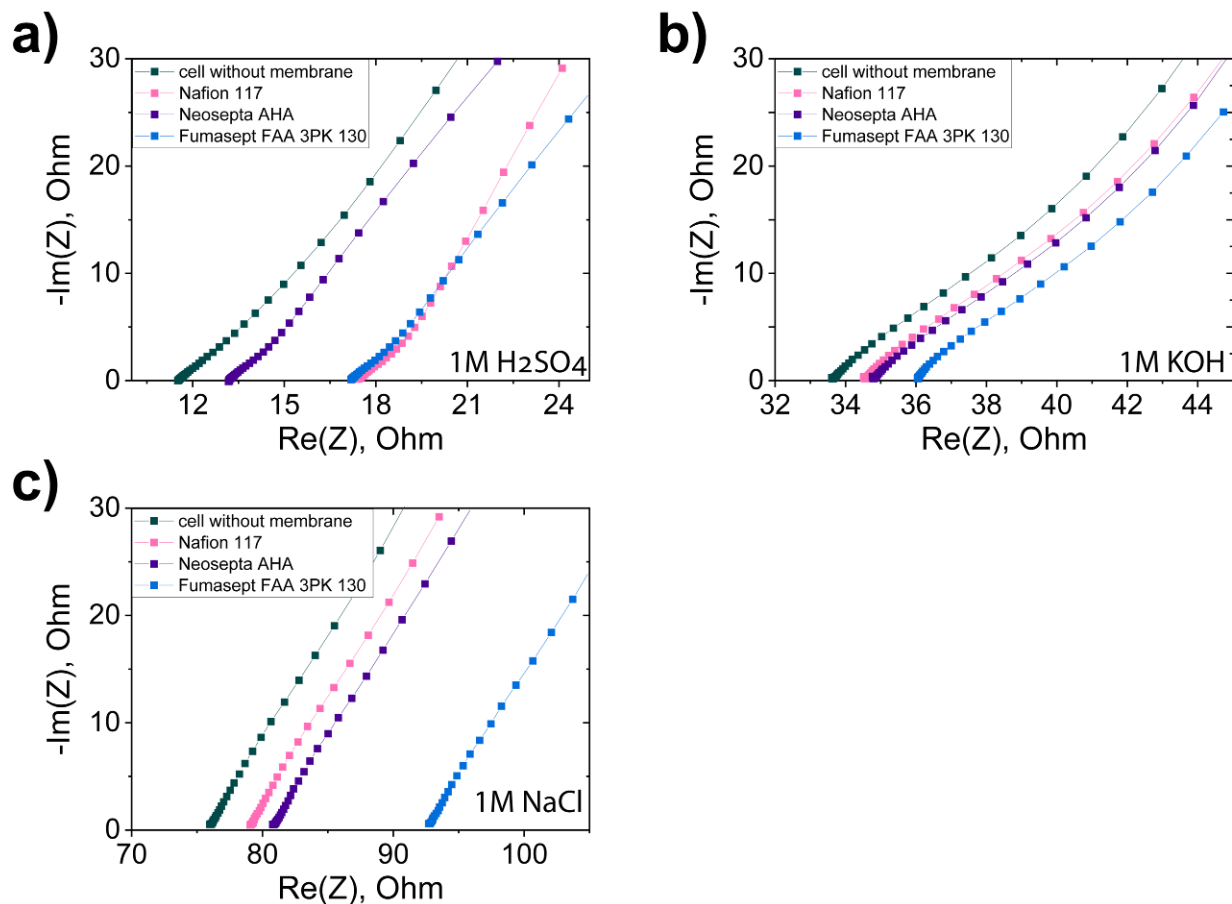


Figure S20. The Nyquist Plots of the non-flow cell with different membranes under with different supporting electrolytes **(a)** 1.0 M H_2SO_4 , **(b)** 1.0 M KOH, **(c)** 1.0 M NaCl.

14. CV of M1 and TEMPOL in neutral conditions

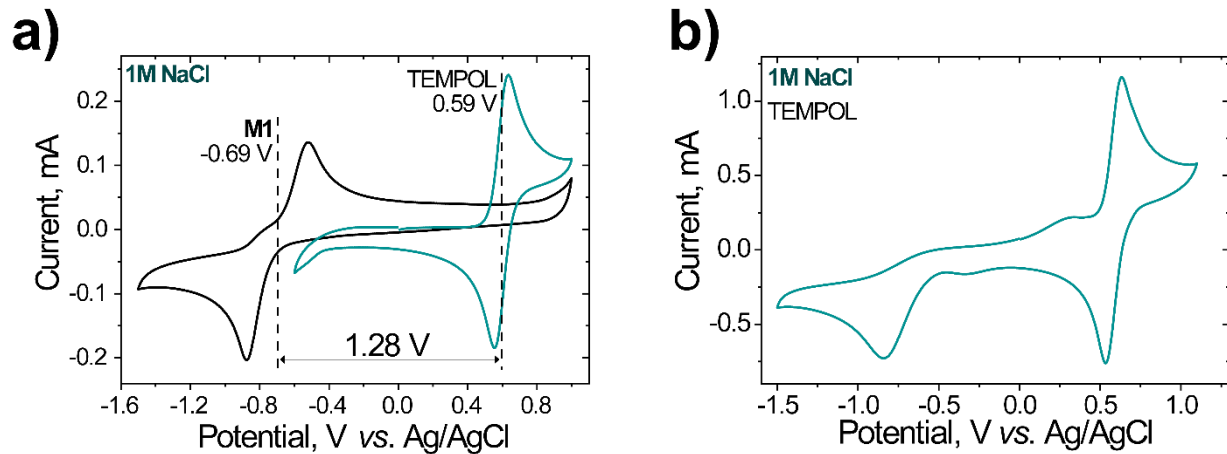


Figure S21. Cyclic voltammograms of pure **M1** (long potential range) and TEMPOL; **(b)** Cyclic voltammograms of pure TEMPOL (long potential range).

15. Investigation of the h-cell with Nafion 117 membrane in neutral conditions

h-cell, Nafion 117 membrane, unmixed electrolytes

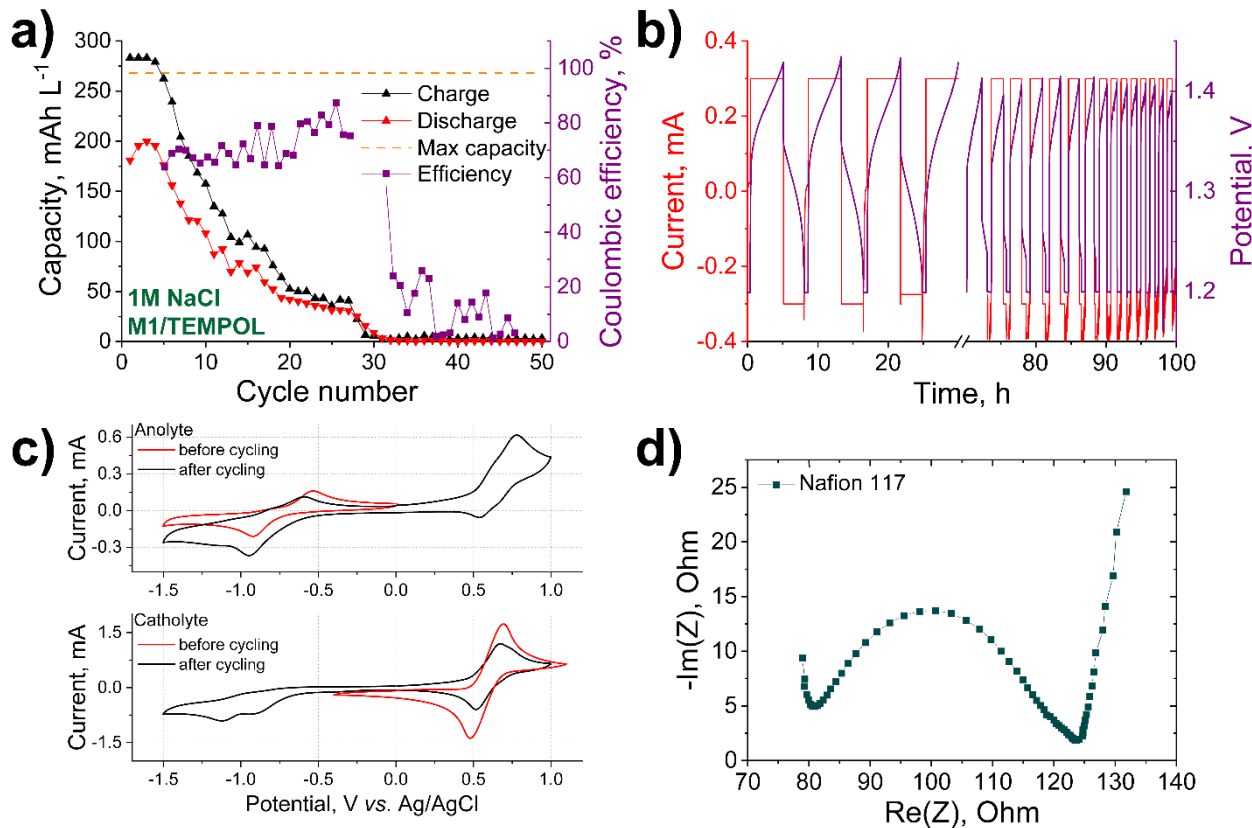


Figure S22. (a) Evolution of the Coulombic efficiency, charge and discharge capacities upon charge-discharge cycling of the h-cell based on **M1** anolyte and TEMPOL catholyte in 1M NaCl water solution with Nafion 117 membrane (unmixed electrolytes were used); (b) Cell voltage and cell current versus time profile for first 30 hours and 70-100 hours of cycling; (c) CVs of the anolyte and catholyte before and after cycling; (d) The Nyquist Plot of the redox flow battery after cycling.

Electrolyte's composition: mixed electrolytes, **M1** – 5.0 mM, **TEMPOL** -50.0 mM, NaCl – 1.0 M in deionised water. Battery charging and discharging time was limited to 18 000 seconds, that is 108% of theoretical battery capacity.

16. Investigation of the h-cell with Fumasept FAA-3PK-130 membrane in neutral conditions

h-cell, Fumasept FAA-3PK-130 membrane, unmixed electrolytes

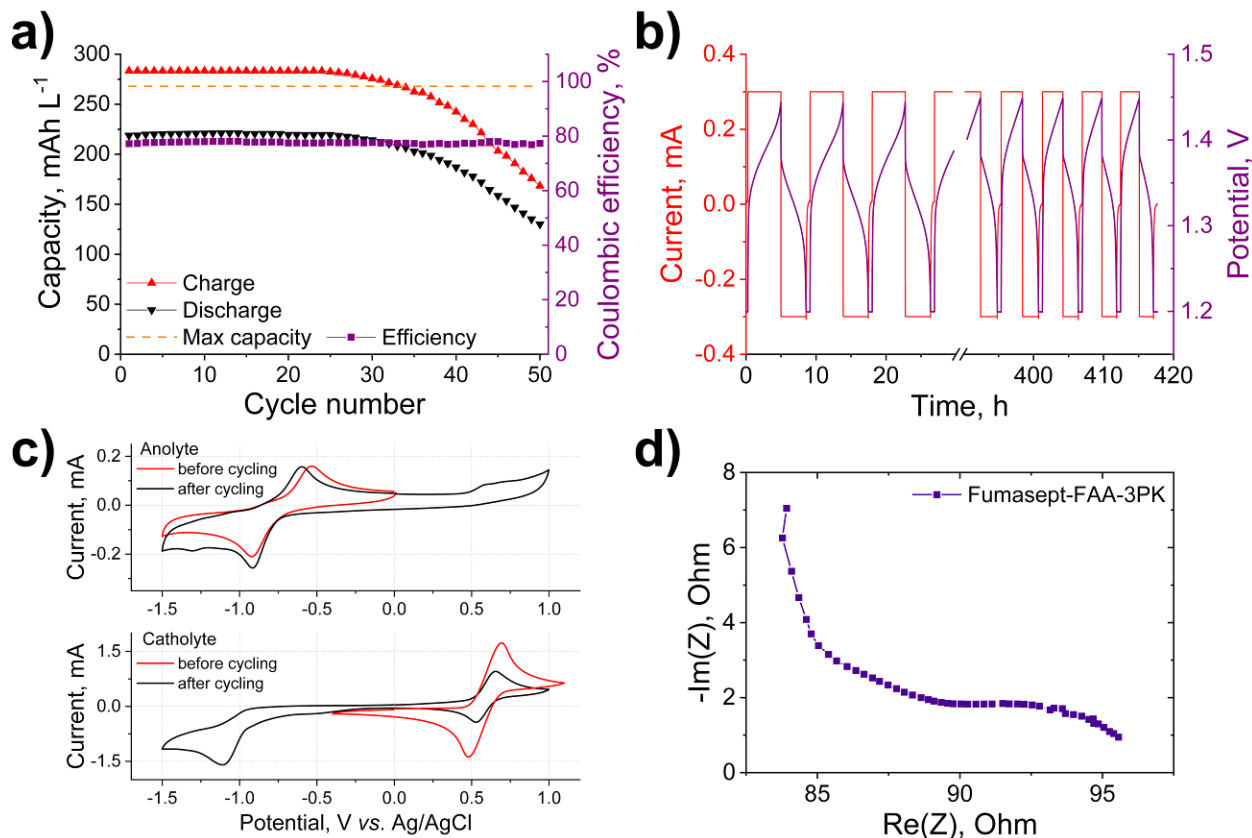


Figure S23. (a) Evolution of the Coulombic efficiency, charge and discharge capacities upon charge-discharge cycling for the h-cell based on M1 anolyte and TEMPOL catholyte in 1M NaCl water solution with Fumasept FAA-3PK-130 membrane (unmixed electrolytes were used); (b) Cell voltage and cell current versus time profile for first 30 hours and 390-420 hours of cycling; (c) CVs of the anolyte and catholyte before and after cycling; (d) The Nyquist Plot of the redox flow battery after cycling.

Electrolyte's composition: mixed electrolytes, **M1** – 5.0 mM, **TEMPOL** -50.0 mM, NaCl – 1.0 M in deionised water. Battery charging and discharging time was limited to 18 000 seconds, that is 108% of theoretical battery capacity.

17. Investigation of the h-cell with Neosepta AHA membrane in neutral conditions

h-cell, Neosepta AHA membrane, unmixed electrolytes

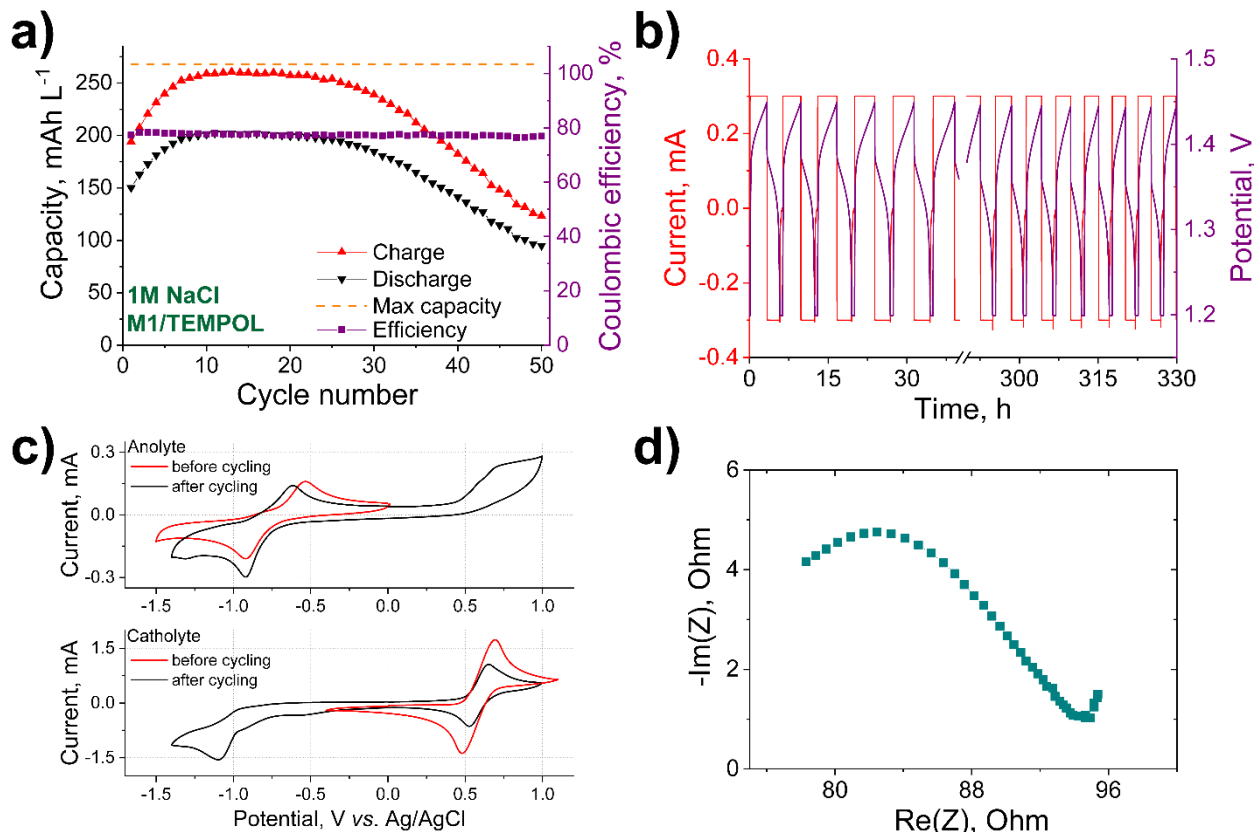


Figure S24. **(a)** Evolution of the Coulombic efficiency, charge and discharge capacities upon charge-discharge cycling for the h-cell based on **M1** anolyte and **TEMPOL** catholyte in **1M NaCl** water solution with Neosepta AHA membrane (unmixed electrolytes were used); **(b)** Cell voltage and cell current versus time profile for first 40 hours and 190-330 hours of cycling; **(c)** CVs of the anolyte and catholyte after cycling; **(d)** The Nyquist Plot of the redox flow battery after cycling.

Electrolyte's composition: mixed electrolytes, **M1** – 5.0 mM, **TEMPOL** -10.0 mM, NaCl – 1.0 M in deionised water. Battery charging and discharging time was limited to 18 000 seconds, that is 108% of theoretical battery capacity.

18. Investigation of the RFB based on M1 anolyte in neutral conditions

RFB, Neosepta AHA membrane, unmixed electrolytes

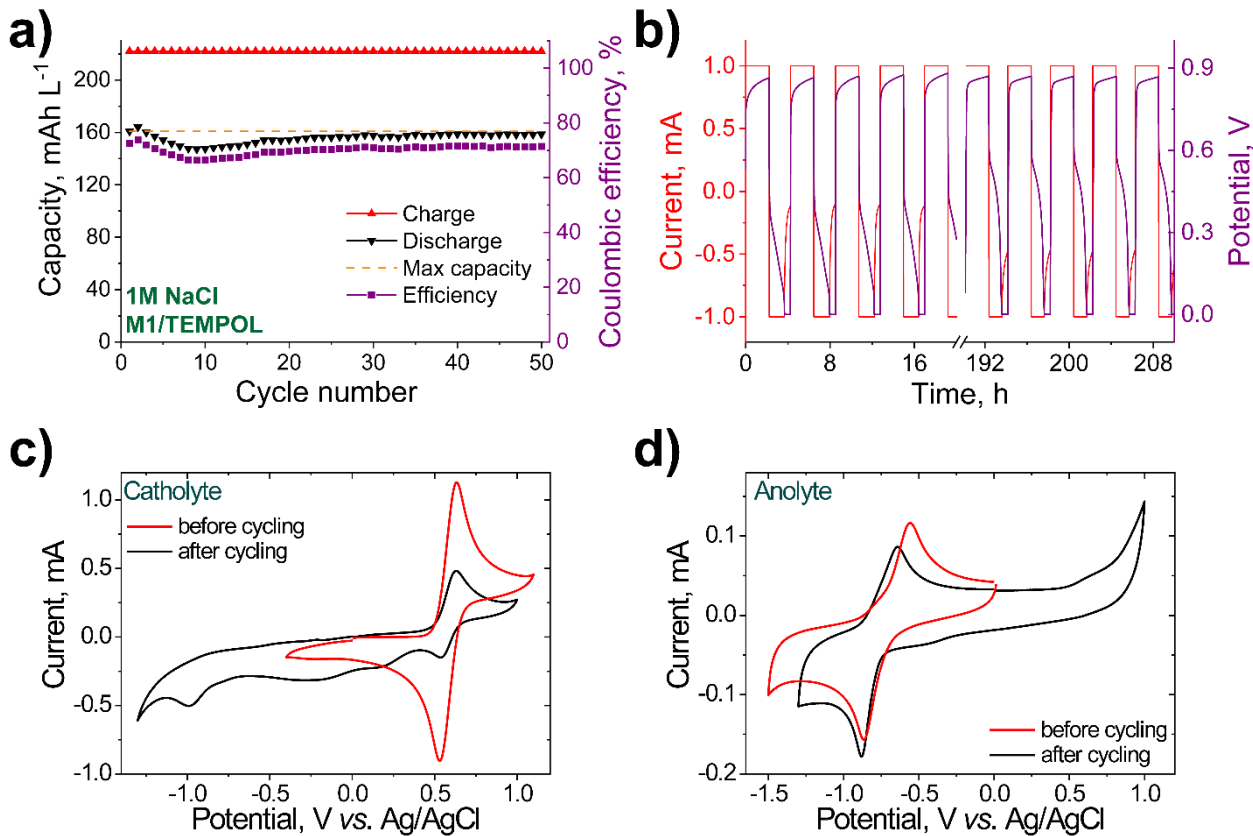


Figure S25. (a) Evolution of the Coulombic efficiency, charge and discharge capacities upon charge-discharge cycling for the redox flow battery based on M1 anolyte and TEMPOL catholyte in 1M NaCl water solution with Neosepta AHA membrane and unmixed electrolytes; (b) Cell voltage and cell current versus time profile for first 20 hours and 190-210 hours of cycling; CVs of the catholyte (c) and anolyte (d) before and after cycling.

Electrolyte's composition: mixed electrolytes, M1 – 3.0 mM, TEMPOL -30.0 mM, NaCl – 1.0 M in deionised water. Battery charging and discharging time was limited to 8000 seconds, that is 138% of theoretical battery capacity.

19. Investigation of the long cycling stability of the RFB based on M1 anolyte in neutral conditions

RFB, Neosepta AHA membrane, unmixed electrolytes

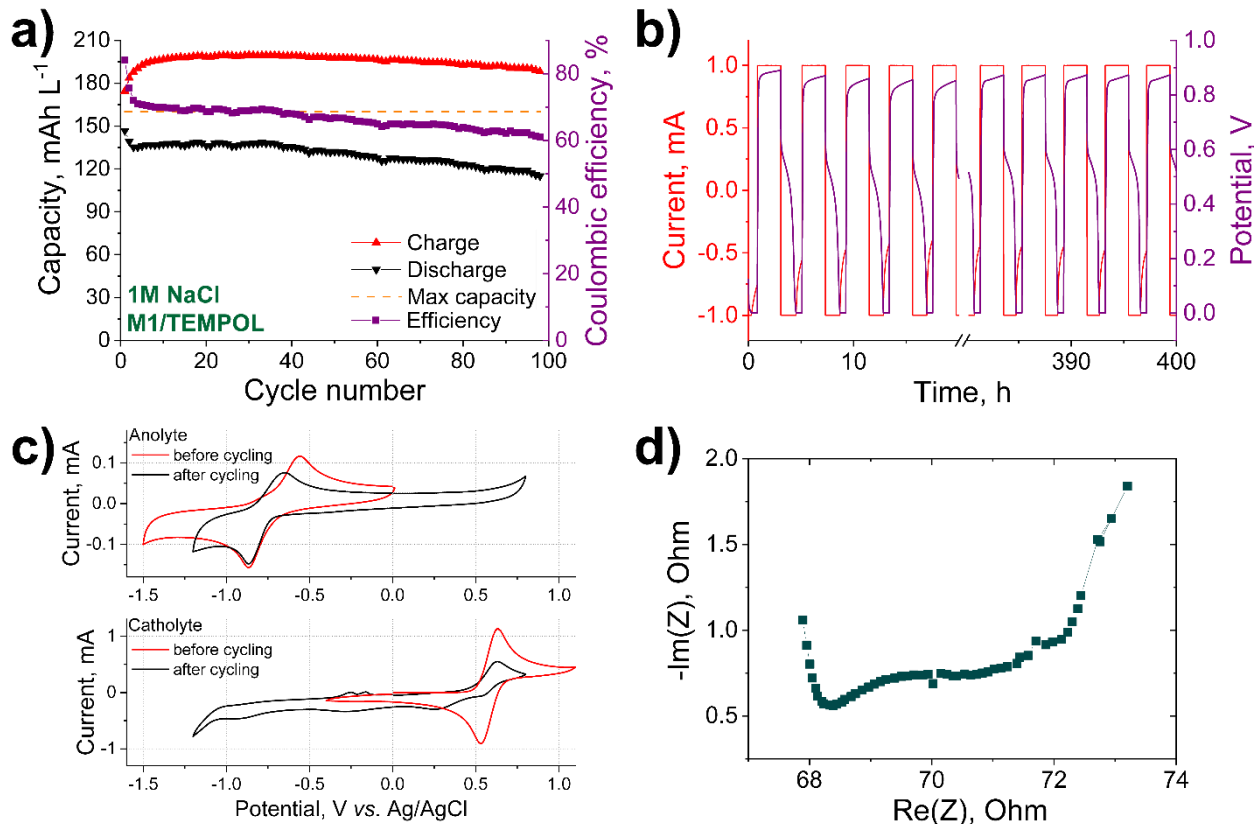


Figure S26. (a) Evolution of the Coulombic efficiency, charge and discharge capacities upon charge-discharge cycling for the redox flow battery based on **M1** anolyte and TEMPOL catholyte in 1M NaCl water solution with Neosepta AHA membrane and unmixed electrolytes; (b) Cell voltage and cell current versus time profile for first 20 hours and 190–210 hours of cycling; (c) CVs of the anolyte and catholyte before and after cycling; (d) The Nyquist Plot of the redox flow battery after cycling.

Electrolyte's composition: mixed electrolytes, **M1** – 3.0 mM, **TEMPOL** -30.0 mM, NaCl – 1.0 M in deionised water. Battery charging and discharging time was limited to 8000 seconds, that is 138% of theoretical battery capacity.

20. CV of M1 and K₄Fe(CN)₆ in base conditions

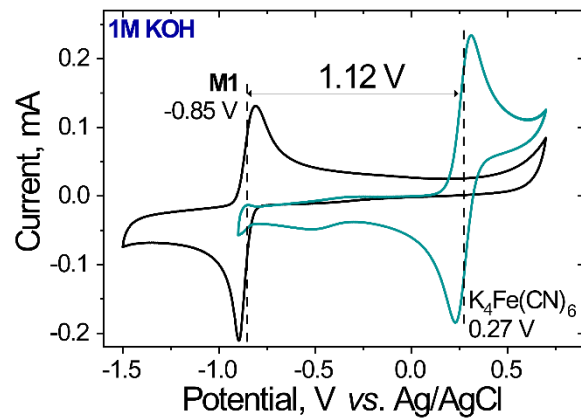


Figure S27. Cyclic voltammograms of pure **M1** and K₄Fe(CN)₆.

21. Investigation of the h-cell based on M1 anolyte in basic conditions upon potentiostatic cycling

h-cell, Neosepta AHA membrane, unmixed electrolytes

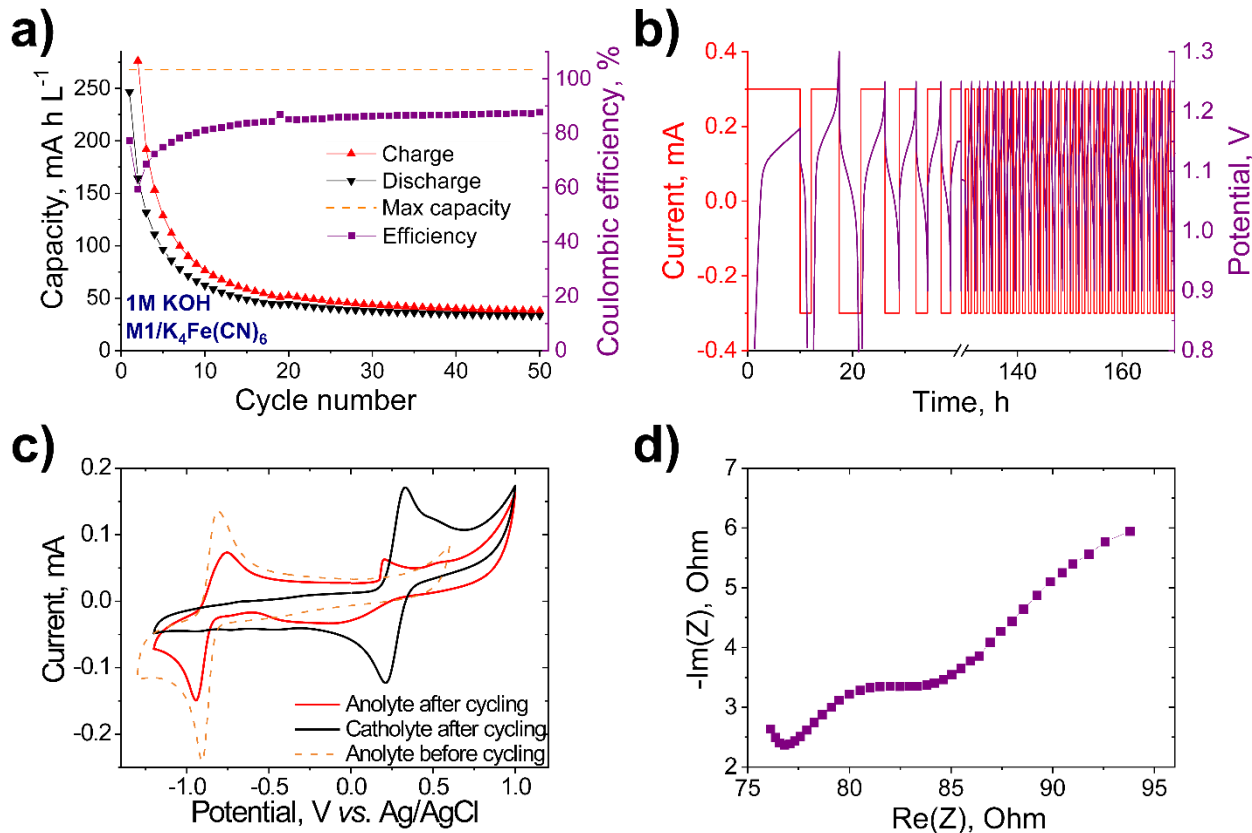


Figure S28. (a) Evolution of the Coulombic efficiency, charge and discharge capacities upon potentiostatic charge-discharge cycling for the h-cell based on **M1** anolyte and $\text{K}_4\text{Fe}(\text{CN})_6$ catholyte in 1M KOH water solution with Neosepta AHA membrane (unmixed electrolytes were used); (b) Cell voltage and cell current versus time profile for first 30 hours and 140-170 hours of cycling; (c) CVs of the catholyte after cycling and anolyte before and after cycling; (d) The Nyquist Plot of the h-cell after cycling.

Electrolyte's composition: anolyte **M1** – 5.0 mM, KOH – 1.0 M in deionised water; catholyte $\text{K}_4\text{Fe}(\text{CN})_6$ – 15 mM, $\text{K}_3\text{Fe}(\text{CN})_6$ – 7.5 mM, KOH – 1.0 M in deionised water.

22. Investigation of the h-cell based on M1 anolyte in basic conditions upon mixed potentiostatic + galvanostatic cycling

h-cell, Neosepta AHA membrane, unmixed electrolytes

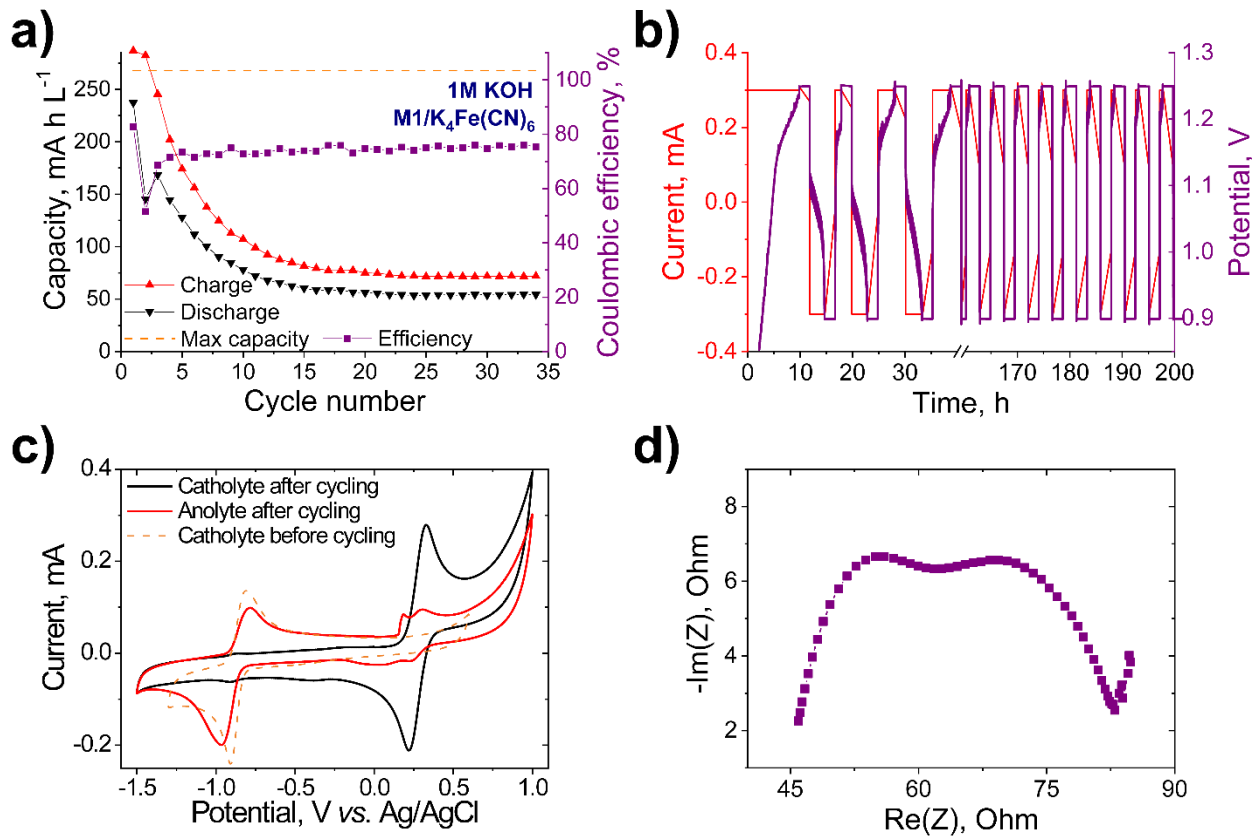


Figure S29. (a) Evolution of the Coulombic efficiency, charge and discharge capacities upon mixed potentiostatic + galvanostatic charge-discharge cycling for the h-cell based on **M1** anolyte and $\text{K}_4\text{Fe}(\text{CN})_6$ catholyte in 1M KOH water solution with Neosepta AHA membrane and unmixed electrolytes; (b) Cell voltage and cell current versus time profile for first 40 hours and 160-200 hours of cycling; (c) CVs of the catholyte after cycling and anolyte before and after cycling; (d) The Nyquist Plot of the h-cell after cycling.

Electrolyte's composition: anolyte **M1** – 5.0 mM, KOH – 1.0 M in deionised water; catholyte $\text{K}_4\text{Fe}(\text{CN})_6$ – 15 mM, $\text{K}_3\text{Fe}(\text{CN})_6$ – 7.5 mM, KOH – 1.0 M in deionised water.

23. Investigation of the h-cell based on M1 anolyte in acidic conditions upon potentiostatic cycling

h-cell, Neosepta AHA membrane, unmixed electrolytes

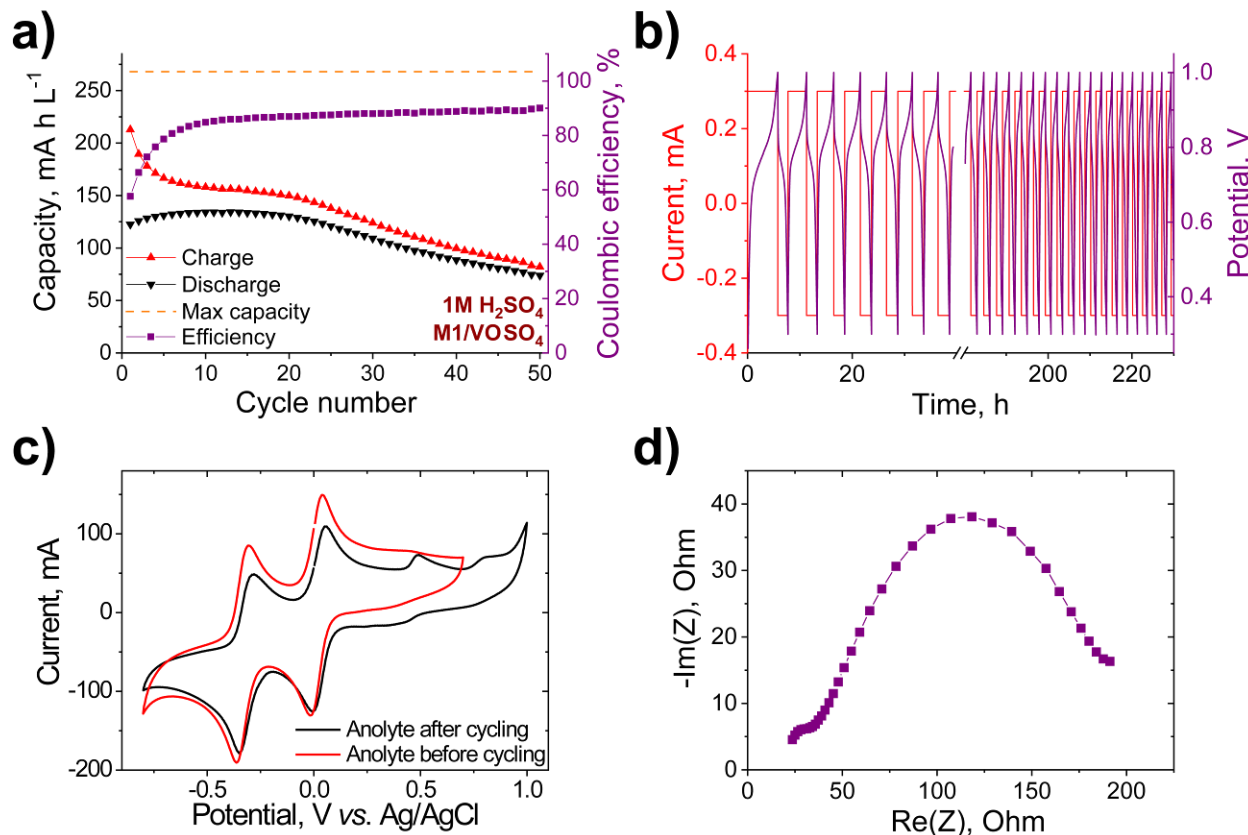


Figure S30. (a) Evolution of the Coulombic efficiency, charge and discharge capacities upon potentiostatic charge-discharge cycling for the h-cell based on **M1** anolyte and VOSO₄ catholyte in 1M H₂SO₄ water solution with Neosepta AHA membrane and unmixed electrolytes; (b) Cell voltage and cell current versus time profile for first 30 hours and 200–230 hours of cycling; (c); CVs of the anolyte before and after cycling; (d) The Nyquist Plot of the h-cell after cycling.

Electrolyte's composition: anolyte **M1** – 5.0 mM, H₂SO₄ – 1.0 M in deionised water; catholyte VOSO₄ – 15 mM, H₂SO₄ – 1.0 M in deionised water.

24. Investigation of the h-cell based on M1 anolyte in acidic conditions upon mixed potentiostatic + galvanostatic cycling

h-cell, Neosepta AHA membrane, unmixed electrolytes

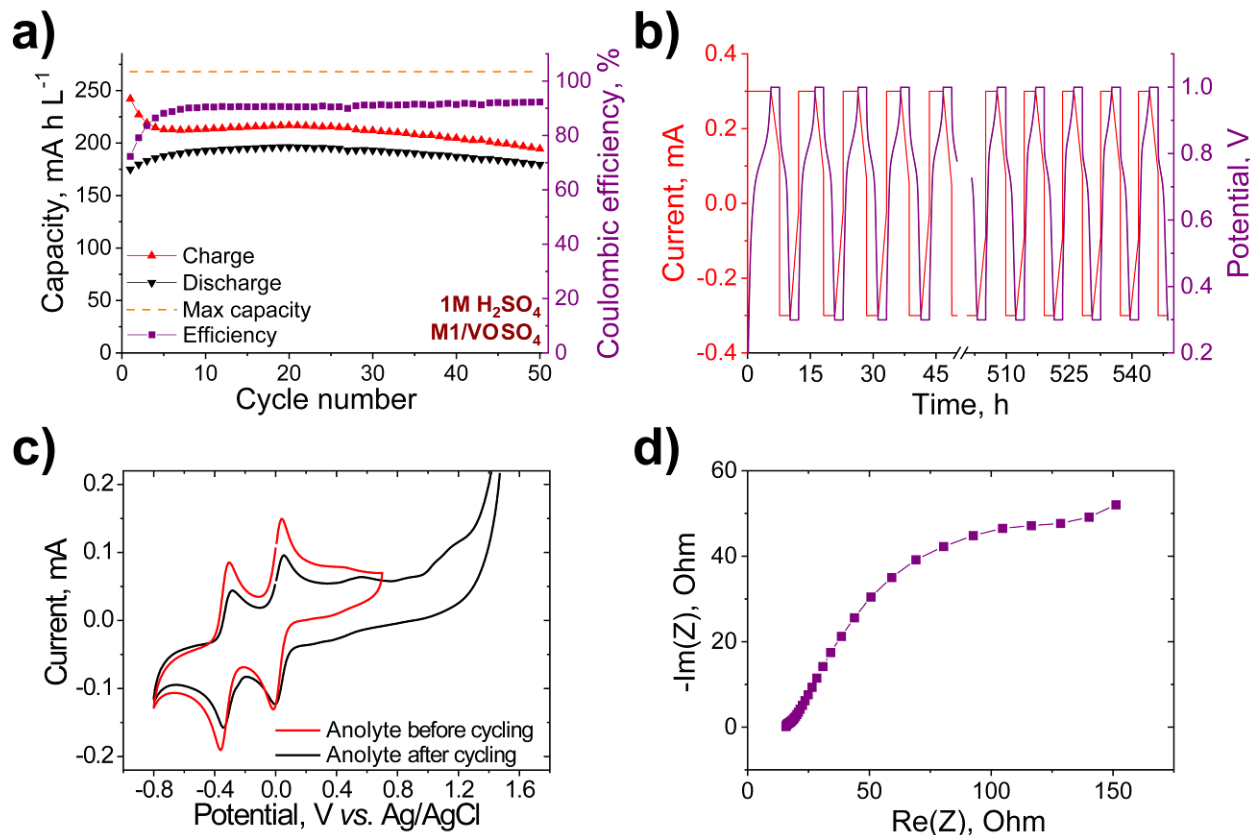


Figure S31. (a) Evolution of the Coulombic efficiency, charge and discharge capacities upon mixed potentiostatic + galvanostatic charge-discharge cycling for the h-cell based on **M1** anolyte and VOSO_4 catholyte in $1\text{M H}_2\text{SO}_4$ water solution with Neosepta AHA membrane and unmixed electrolytes; (b) Cell voltage and cell current versus time profile for first 40 hours and 510-550 hours of cycling; (c) CVs of the anolyte before and after cycling; (d) The Nyquist Plot of the the h-cell after cycling.

Electrolyte's composition: anolyte **M1** – 5.0 mM, H_2SO_4 – 1.0 M in deionised water; catholyte VOSO_4 – 15 mM, H_2SO_4 – 1.0 M in deionised water.

25. Investigation of the h-cell based on M1 anolyte in acidic conditions under different charge-discharge currents

h-cell, Neosepta AHA membrane, unmixed electrolytes

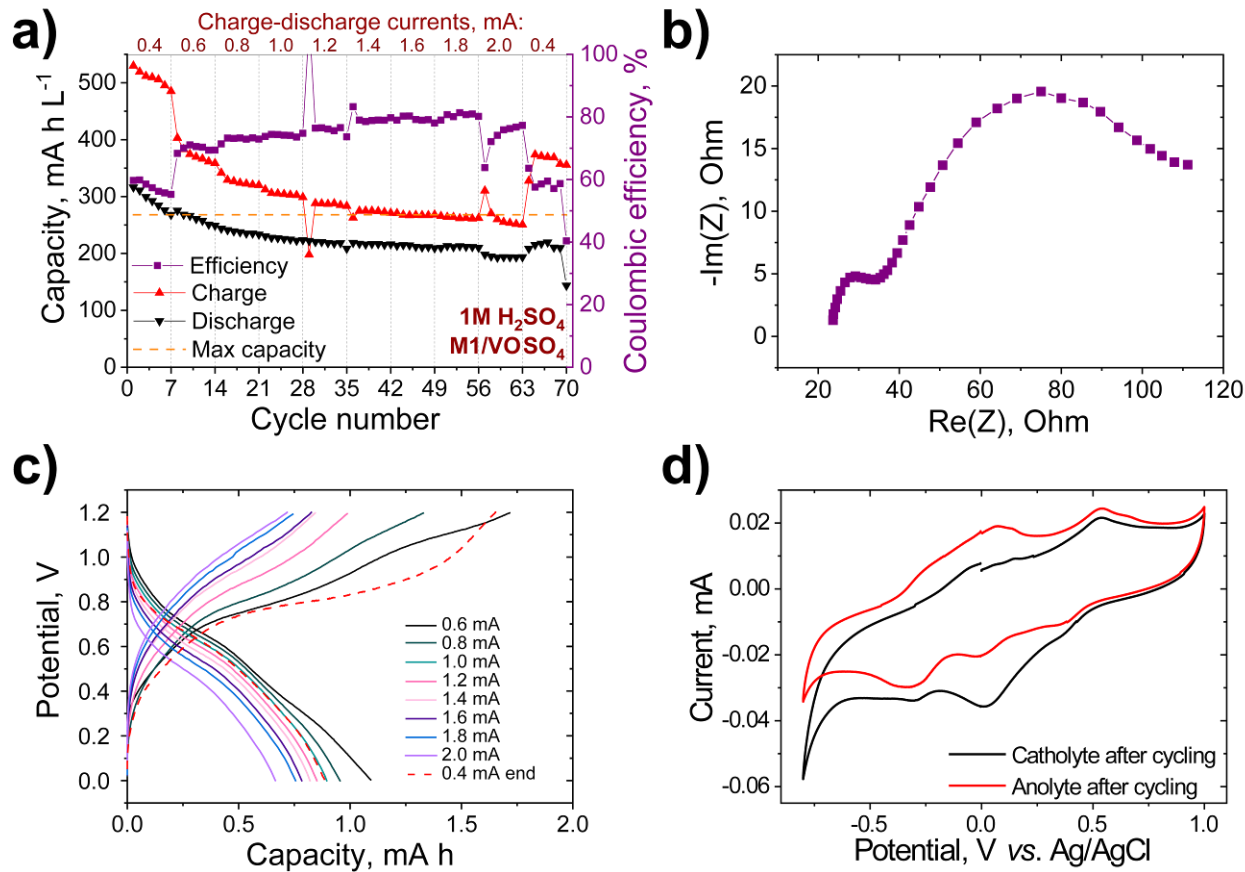


Figure S32. **(a)** Evolution of the Coulombic efficiency, charge and discharge capacities upon charge-discharge cycling at the different currents for the h-cells based on **M1** anolyte, VOSO₄ catholyte in 1M H₂SO₄ water solution with Neosepta AHA membrane; **(b)** The Nyquist Plot of the the h-cell after cycling; **(c)** Evolution of the charge and discharge capacities upon charge-discharge cycling at the different currents for the h-cells based on **M1** anolyte, VOSO₄ catholyte in 1M H₂SO₄ water solution with Neosepta AHA membrane; **(d)** CVs of the anolyte and catholyte after cycling.

Electrolyte's composition: anolyte **M1** – 5.0 mM, H₂SO₄ – 1.0 M in deionised water; catholyte VOSO₄ – 15 mM, H₂SO₄ – 1.0 M in deionised water.

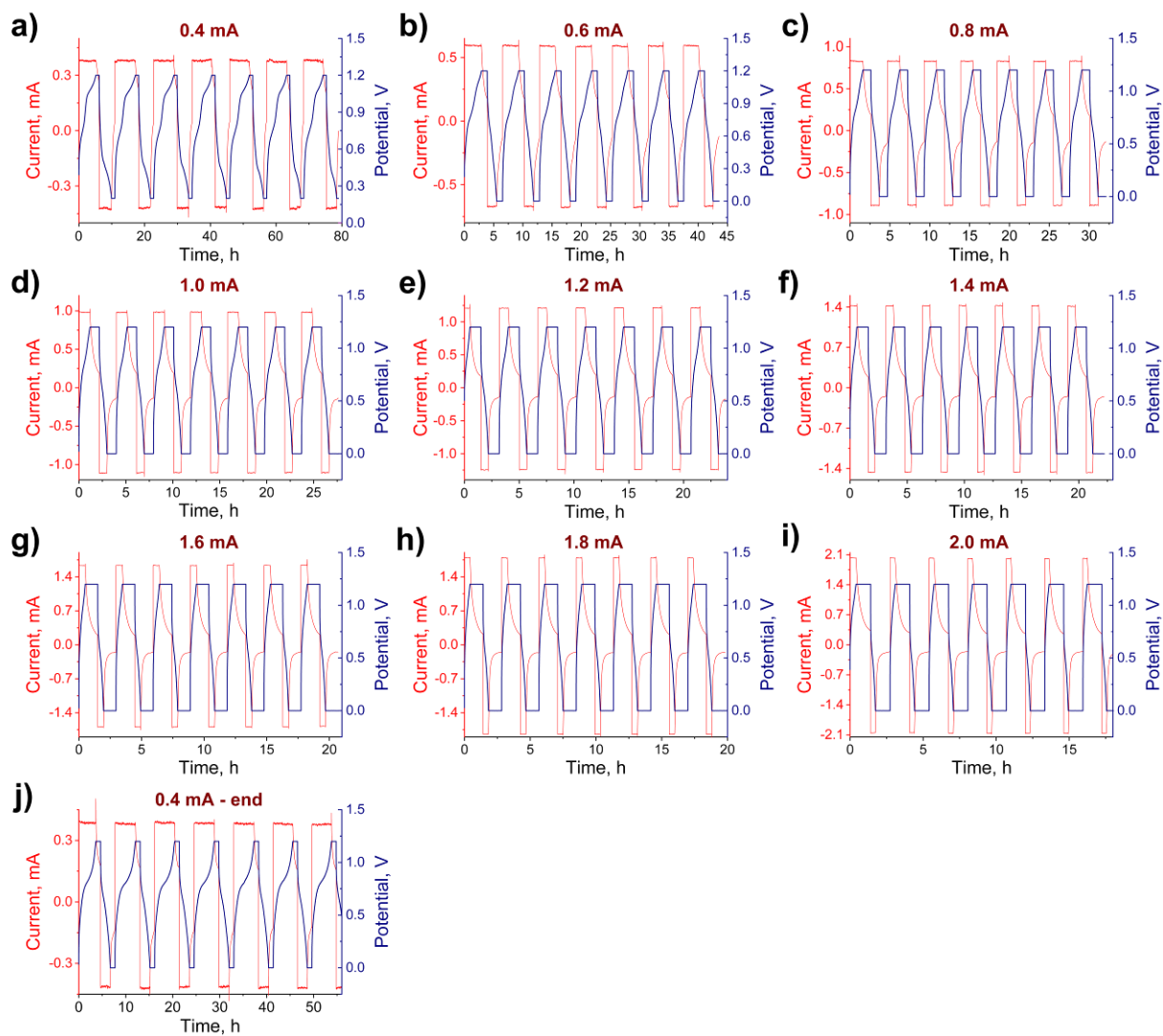


Figure S33. Potential-time dependence curves for the h-cell cycling based on **M1** anolyte, VOSO₄ catholyte in 1M H₂SO₄ water solution with Neosepta AHA membrane under different charge-discharge currents: **(a)** 0.4 mA, **(b)** 0.6 mA, **(c)** 0.8 mA, **(d)** 1.0 mA, **(e)** 1.2 mA, **(f)** 1.4 mA, **(g)** 1.6 mA, **(h)** 1.8 mA, **(i)** 2.0 mA, **(j)** 0.4 mA return to the starting value.

26. Investigation of the cycling stability of the RFB with Neosepta AHA membrane in acidic conditions

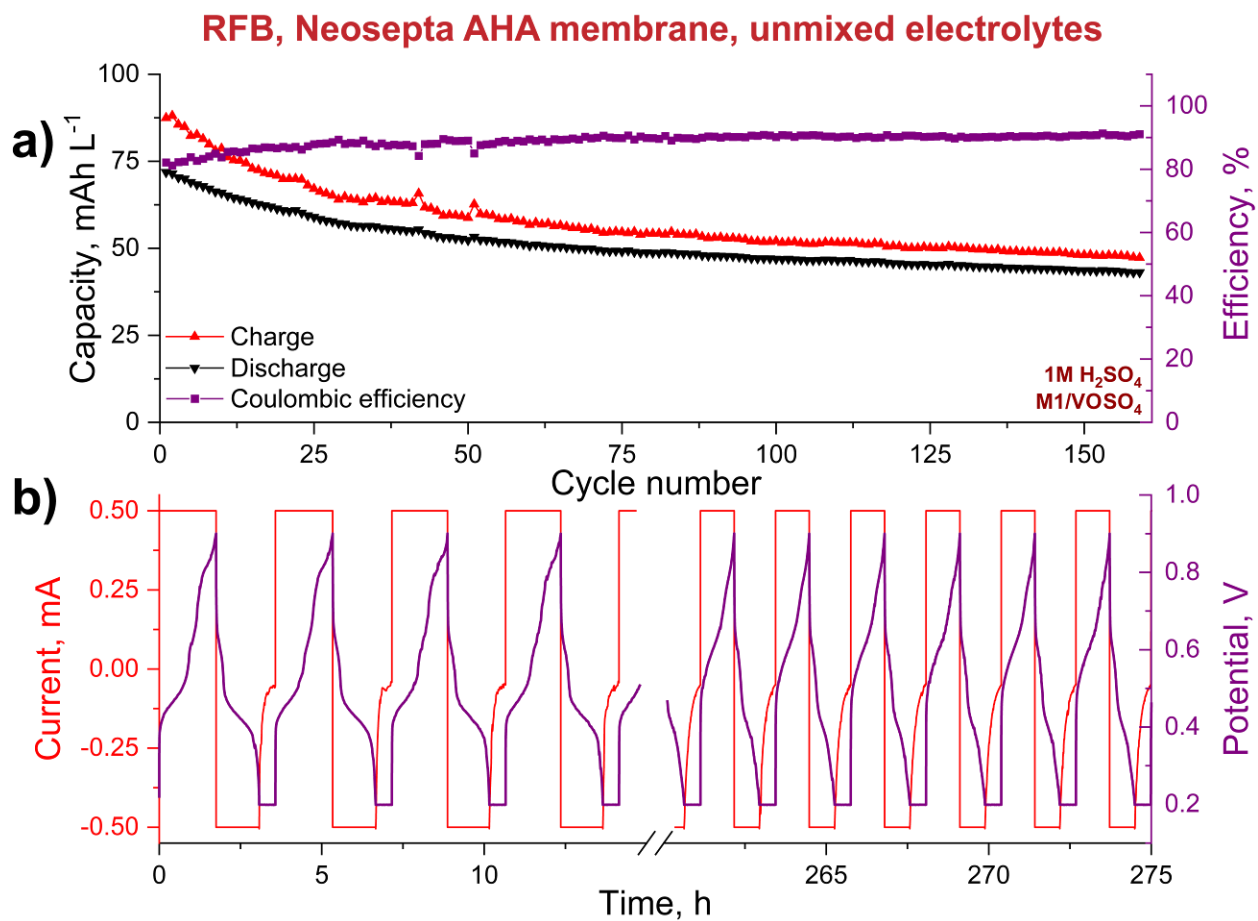


Figure S34. (a) Evolution of the Coulombic efficiency, charge and discharge capacities upon mixed potentiostatic + galvanostatic charge-discharge cycling for the h-cell based on **M1** anolyte and VOSO_4 catholyte in $1\text{M H}_2\text{SO}_4$ water solution with Neosepta AHA membrane and unmixed electrolytes; (b) Cell voltage and cell current versus time profile for first 20 hours and 255-275 hours of cycling.

Electrolyte's composition: anolyte **M1** – 3.0 mM, H_2SO_4 – 1.0 M in deionised water; catholyte VOSO_4 – 10 mM, H_2SO_4 – 1.0 M in deionised water.

27. Investigation of the long cycling stability of the RFB with Neosepta AHA membrane in acidic conditions

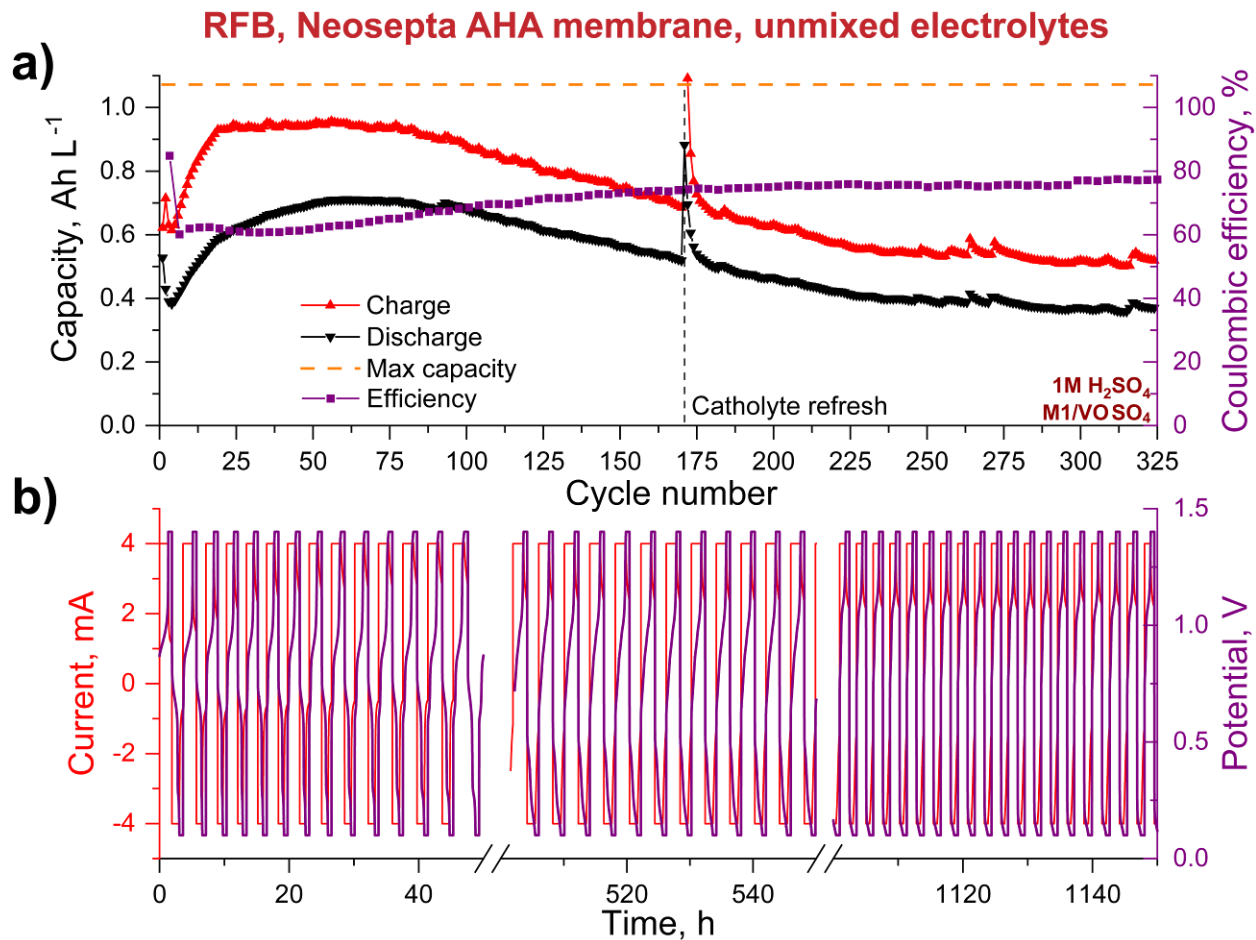


Figure S35. (a) Evolution of the Coulombic efficiency, charge and discharge capacities upon mixed potentiostatic + galvanostatic charge-discharge cycling for the RFB based on **M1** anolyte and VOSO_4 catholyte in 1M H_2SO_4 water solution with Neosepta AHA membrane and unmixed electrolytes; (b) Cell voltage and cell current versus time profile for first 50 hours, 500-550 hours and 1100-1150 hours of cycling.

Electrolyte's composition: anolyte **M1** – 20.0 mM, H_2SO_4 – 1.0 M in deionised water; catholyte VOSO_4 – 60 mM, H_2SO_4 – 1.0 M in deionised water.

References

- [S1] Hollas A.; Wei X.; Murugesan V.; Nie Z.; Li B.; Reed D.; Liu J.; Sprenkle V.; Wang W., A biomimetic high-capacity phenazine-based anolyte for aqueous organic redox flow batteries, *Nat. Energy*, **2018**, *3*, 508–514, doi: 10.1038/s41560-018-0167-3. 50
- [S2] Phenazine | C₁₂H₈N₂ - PubChem, <https://pubchem.ncbi.nlm.nih.gov/compound/Phenazine>, (accessed 28 October 2022). 72 UBACENO
- [S3] Romadina, E.I.; Komarov, D.S.; Stevenson, K.J.; Troshin, P.A. New Phenazine Based Anolyte Material for High Voltage Organic Redox Flow Batteries. *Chem. Commun.* **2021**, *57*, 2986–2989, doi:10.1039/D0CC07951K. 54
- [S4] Lai, Y.Y.; Li, X.; Liu, K.; Tung, W.Y.; Cheng, C.F.; Zhu, Y. Stable Low-Cost Organic Dye Anolyte for Aqueous Organic Redox Flow Battery. *ACS Appl. Energy Mater.* **2020**, *3*, 2290–2295, doi:10.1021/acsaem.9b01735. 14
- [S5] Hong J.; Kim K.; Neutral Red and Ferroin as Reversible and Rapid Redox Materials for Redox Flow Batteries, *ChemSusChem*, **2018**, *11*, 1866–1872, doi: 10.1002/cssc.201800303 73 UBACENO
- [S6] Wang, C.; Li, X.; Yu, B.; Wang, Y.; Yang, Z.; Wang, H.; Lin, H.; Ma, J.; Li, G.; Jin, Z. Molecular Design of Fused-Ring Phenazine Derivatives for Long-Cycling Alkaline Redox Flow Batteries. *ACS Energy Lett.* **2020**, *5*, 411–417, doi:10.1021/acsenergylett.9b02676. 51
- [S7] Pang, S.; Wang, X.; Wang, P.; Ji, Y. Biomimetic Amino Acid Functionalized Phenazine Flow Batteries with Long Lifetime at Near-Neutral PH. *Angew. Chemie - Int. Ed.* **2021**, *60*, 5289–5298, doi:10.1002/anie.202014610. 52
- [S8] Xu, J.; Pang, S.; Wang, X.; Wang, P.; Ji, Y. Ultrastable Aqueous Phenazine Flow Batteries with High Capacity Operated at Elevated Temperatures. *Joule* **2021**, *5*, 2437–2449, doi:10.1016/j.joule.2021.06.019. 49
- [S9] Winsberg, J.; Stolze, C.; Muench, S.; Liedl, F.; Hager, M.D.; Schubert, U.S. TEMPO/Phenazine Combi-Molecule: A Redox-Active Material for Symmetric Aqueous Redox-Flow Batteries. *ACS Energy Lett.* **2016**, *1*, 976–980, doi:10.1021/acsenergylett.6b00413. 52
- [S10] Wellala N.; Hollas A.; Duanmu K.; Murugesan V.; Zhang X.; Feng R.; Shao Y.; Wang W., Decomposition pathways and mitigation strategies for highly-stable hydroxyphenazine flow battery anolytes, *J. Mater. Chem. A*, **2021**, *9*, 21918–21928. doi: 10.1039/D1TA03655F. 74 UBACENO
- [S11] Safety data sheet “Potassium Hydroxide, 0.5N (0.5M)”, according to Federal Register, 77 (58) March 26, **2012**, Rules and Regulations
- [S12] Rhodes F.; Barbour C.; The Viscosities of Mixtures of Sulfuric Acid and Water, *Ind. Eng. Chem.*, **1923**, *15*, 850–852. doi: 10.1021/ie50164a033